Universidade de Aveiro
Ano 2013/2014

Departamento de Engenharia de Materiais e Cerâmica

Hugues Mondésert

Mineralização de nanofibras de PLGA para regeneração periodontal

Mineralization of PLGA nanofibers for periodontal tissue regeneration

Dissertação apresentada à Universidade de Aveiro para cumprimento dos requisitos necessários à obtenção do grau de Mestre em Ciência e Engenharia de materiais, realizada sob a orientação científica da Doutora Kerstin Gritsch[1], da Doutora Doris Campos[1], do Doutor Jérôme Sohier[2], da Doutora Elisabete Costa[3] a da Doutora Brigitte Grosgogeat[1].

[1] Laboratoire des Multimatériaux et des Interfaces Biologiques (UMR CNRS 5615), Université Claude Bernard Lyon 1

[2] Institut de Biologie et de Chimie des Protéines (IBCP), Université Claude Bernard Lyon 1

[3] Universidade de Aveiro

FAME Master Thesis 2014

O júri

Presidente — Ana Margarida Madeira Viegas de Barros Timmons
Professora Auxiliar do Departamento de Química da Universidade de Aveiro

Paula Alexandrina de Aguiar Pereira Marques
Investigadora Principal do Departamento de Engenharia Mecânica da Universidade de Aveiro

Maria Elizabete Jorge Vieira da Costa
Professora Auxiliar do Departamento de Engenharia de Materiais e Cerâmica da Universidade de Aveiro

Agradecimentos

Foremost, I would like to express my sincere gratitude to my professors and coordinators in the University of Aveiro, Dr. Elisabete Costa and Dr. Ana Barros for the support of my master thesis research program, for their patience, motivation and enthusiasm. I would like thank them for their reactive and available behaviours regarding the organisation and administrative procedures between France and Portugal.

I would like to thank my supervisors in France, Dr. Kerstin Gritsch, Dr. Doris Moura Campos, Dr. Jérôme Sohier and Dr. Brigitte Grosgogeat for the guidance of my master thesis, their trust, encouragement and very interesting comments and advices they gave me.

My sincere thanks goes to Dr. Doris Moura Campos, who made me feel welcome in the laboratory and guided me in my first writings. Thank you to Dr. Jérôme Sohier for his availability and for sharing his knowledge on Jet Spraying technique.

I would like to thank my labmate Diego Garcia Miranda for his crucial help in biology field, Bruno Gardiola for XRD measurements and my labmates AliceFerrand, Hazem Hassan Abouelleil, Nina Attik, Kadiatou Sy and Hallay Frank for the stimulating discussions we had during these 5 months.

Thank you to Mikalai Zhuk and Kyle Debelak for all the moments we shared in Aveiro, Portuguese classes, hambergurs especiais and the coffee discussions.

Last but not the least, I would like to thank my family: my parents Gentil-Mondésert Sylvie and Mondésert François and my two brothers Grégoire and Étienne, for always supporting me spiritually throughout my life.

Palavras-chave

Engenharia de tecidos, regeneração periodontal, mineralização, electrofiacção, pulverização por jacto , fluido humano simulado.

Resumo

A doença periodontal induz uma inflamação que pode levar à destruição dos tecidos de suporte do dente. A degradação provocada pela doença pode ser tratada com o recurso a suportes sintéticos que permitam a regeneração progressiva dos tecidos. As nanofibras de ácido polilactico co-glicolico (PLGA), mineralizadas, produzidas por electrofiação ou pela técnica de pulverização por jacto, são biomateriais adequados para funcionarem como suporte físico temporário e assegurarem a biocompatibilidade necessária à regeneração de tecidos. O presente trabalho tem como objetivo o estudo da mineralização de nano-fibras de PLGA para optimizar a regeneração de tecidos duros. São propostos dois métodos de mineralização: o método baseado no fluido fisiológico simulado (SBF) e o método baseado na pulverização por jacto (JS). A técnica de SBF consiste em mergulhar matrizes de PLGA, produzidas por electrofiação, numa solução concentrada de sais ao passo que a técnica de JS consiste em pulverizar uma suspensão preparada com nanopartículas de hidroxiapatite ($Ca_5(PO_4)_3(OH)$, HA) e uma solução polimérica.

Os materiais produzidos foram caracterizados por difração de Raios- X (DRX) e por microscopia electrónica de varrimento (MEV). Para as amostras processadas pela técnica de SBF os resultados de DRX evidenciaram a presença de fosfatos de cálcio de baixa cristalinidade, correspondentes à fase de hidroxiapatite. As imagens de MEV permitiram observar a formação de estruturas minerais fortemente dependentes do tempo de imersão. Nas matrizes de PLGA tratadas por JS, a DRX confirmou a presença de HA e a MEV revelou que a morfologia das amostras depende da concentração das nanopartículas de HA adicionadas à solução polimérica inicial. O método de SBF permitiu uma deposição superficial de fosfatos de cálcio ao passo que, pelo método de JS, foi possível incorporar nanopartículas de HA no seio da matriz polimérica. A combinação dos dois métodos parece pois ser uma técnica promissora para fabricar suportes mineralizados para regeneração de tecido periodontal.

Keywords **Tissue engineering, periodontal regeneration, mineralization, electrospinning, jet spraying, Simulated body fluid**.

Abstract

Periodontal diseases induce a loss of soft and hard tissues surrounding the teeth after inflammation. Defects created by the infection would be replaced by the synthetic scaffold allowing progressive tissue regeneration. Mineralized PLGA (poly(lactic-co-glycolic acid)) nanofibers developed by electrospinning or jet spraying techniques are efficient biomaterials to maintain temporarily a physical structure and to enhance biocompatibility for hard tissue regeneration. The aim of this work was to mineralize PLGA nanofibers by two different methods: Simulated Body Fluid (SBF) immersion and projection by jet spraying (JS). SBF method consists in soaking PLGA matrices into high ions concentrated solutions (SBFx1 or SBFx5) to deposit mineral layers. With the new JS technique, we target a formation of a nanocomposite of PLGA and hydroxyapatite nanoparticles (nHA): first with the help of a blend solution (PLGA + nHA) directly projected (JS) and then with a simultaneous co projection of PLGA solution and nHA suspension in water (Co-JS).

From material characterization perspective, samples produced by SBFx1 protocol showed a very weak mineral deposition, low crystalline sodium chloride whereas SBFx5 solutions allowed the formation of a consequent CaP mineral layer on electrospun PLGA matrices. SEM images allowed the observation of different mineral structures strongly depending on SBF concentration and immersion time. XRD patterns confirmed the presence of HA into JS PLGA matrices. Morphologically, JS scaffolds varied with the concentration of HA nanoparticles incorporated into the initial mixture. HA nanoparticles were successfully incorporated inside the polymer fibers with the first Jet spraying technique (JS) whereas nHAs were successfully deposited on the surface of the PLGA fibers with Co JS method.

Table of contents

List of Figures

List of Figures

I - Introduction

Tissue engineering science is currently developing a new generation of implants that could facilitate and target a complete reconstruction of damaged tissues. Tooth hard tissues, named as periodontal tissues, could be seriously damaged by chronic diseases such as periodontitis (1). Current healing techniques do not allow the complete regeneration of these hard tissues which support the teeth. Clinical surgeries only permit the microbiological cleaning of contaminated tissues, forming voids, periodontal pockets, between the tooth and the alveolar bone. A new approach of engineered biomaterials might provide a solution for a complete regeneration *ad integrum* of the periodontium. Polymers nanofibers were developed to construct a scaffold biocompatible with the host environment and trigger an invasion and settling of new cells (2). Cell colonisation and proliferation will ensure a viable reproduction of the External Cellular Matrix (ECM). The synthetic structure works as a temporary support (artificial ECM) allowing the progressive reconstruction of periodontal tissues.

Polymer nanoporous scaffolds such as PLGA nanofibers are now deigned for tissue regeneration applications (3). PLGA has few particular features (biocompatibility, degradation times in accordance with the formation delay of hard tissues, etc…) that make the polymer a good biomaterial for regeneration scaffold. Recent progresses in nanofibers synthesis, mainly through electrospinning and jet spraying techniques, lead to an increase of interest for tissue engineering nanostructured scaffolds.

However, biocompatibility abilities of PLGA nanofibers still have to be enhanced for a complete integration of the implant. In this study, we investigated three approaches to mineralize PLGA nanofibers, with simulated body fluids mineralization, and nanocomposite processing through jet spraying and co jet spraying. The incorporation of calcium phosphate (CaP) minerals inside the PLGA matrices may initiate the *in vivo* mineralization process and improve the global biocompatibility of the synthetic network.

II - Periodontal diseases

Periodontitis is a chronic disease that induces the progressive destruction of the periodontium, which forms the tissues surrounding and supporting the teeth, i.e. gingiva (gum), alveolar bone, periodontal ligament (PDL) and root cementum (see **figure 1**). The development of the inflammation if untreated can deteriorate alveolar bone and lead to loosening and subsequent loss of the teeth.

The disease is caused by the accumulation of microorganisms (harmful bacteria and protozoa) that proliferate at surface of the teeth and provoke an over-aggressive immune response. The four periodontal tissues are progressively damaged if the disease is not treated. Periodontitis could also have major influences on others vascular diseases such as diabetes. The dentist makes the diagnosis by detecting the presence of periodontal pockets (spaces created between the gums and the teeth) and with X-rays analysis to evaluate bone loss (see **figure 1**).

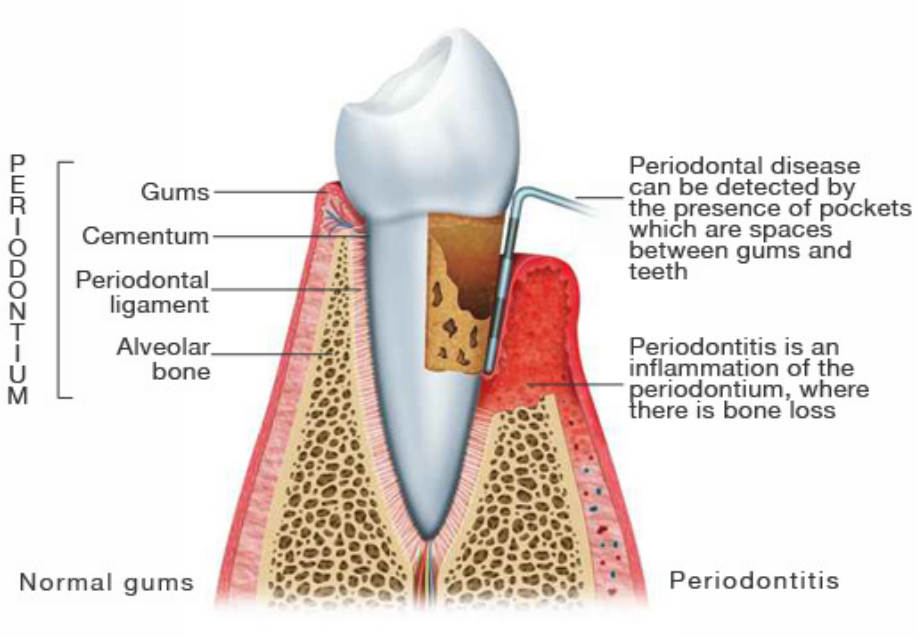

Figure 1 – *Periodontitis disease* (4)

Nowadays, dentists remove and clean the damaged tissues to heal the patient. But no treatments are currently available to regenerate *ad integrum* the lost tissues. Periodontal regeneration, defined as the reproduction or reconstruction of lost or injured tissue so that the lost form and function are restored, has not been successful in humans so far.

The poor ability to the damaged tissues to repair themselves demonstrates the need to develop new efficient regenerative strategies. Tissue engineering proposes a promising alternative in this perspective.

III- Tissue engineering for periodontium regeneration

1) Current method for periodontium regeneration

Several regenerative techniques were developed in order to improve and facilitate the restoration of the lost tissues. In the 1980s, a process called Guided Tissue Regeneration (GTR) was created for guiding bone, cementum and PDL regeneration. The system is composed by a membrane of variable porosity that prevents the growth of the epithelium and the fibroblast recruitment into the pocket formed by the periodontitis. The barrier is positioned as shown on the **figure 2** in such way that it maintains a space for true periodontal tissue regeneration. It separates the superficial periodontium and the deep periodontium maintaining a “free” space for the regeneration of PDL and alveolar bone. Gum tissue grows at a much faster rate than bone; therefore, membranes are used to prevent gum tissue from growing in. It was shown that this technique was efficient only in a few cases where the intra-bony defects are narrow (5). The GTR system could be also coupled to a bone graft that will provide a mechanical support to the tooth replacing the damaged alveolar tissue. The membrane will help and stabilize the bone grafts as well as displace the gum tissue from invading the healing bone graft.

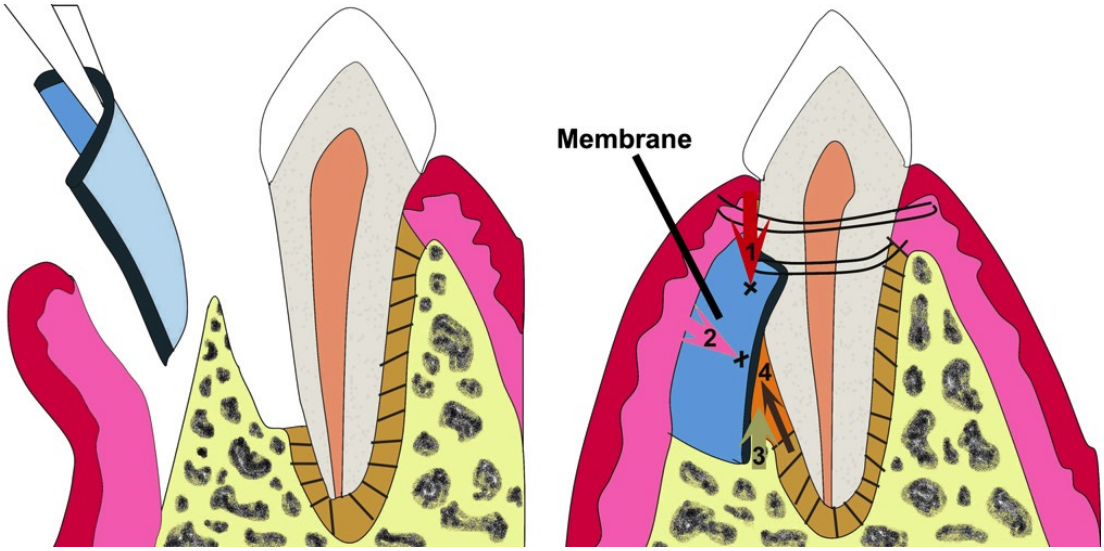

Figure 2 - Guided Tissue Regeneration membrane technique (1)

2) Tissue engineering

Tissue engineering is a new field that combines the principles of biology, engineering and material sciences in view of developing functional substitutes for damaged tissue. This promising field has been studied with great interest in order to build systems to restore, maintain, replace or improve biological functions for the past 20 years (6). The new generation of biomaterials targets a progressive regeneration. A synthetic scaffold provides a temporal support for cellular colonization into the implant site. These temporary frameworks provide a three-dimensional microenvironment where cells can proliferate, differentiate and generate the desired tissue. The progressive regeneration of the damaged tissues optimally corresponds to the progressive biodegradation of the artificial matrix. Cellular interactions play a crucial role in the acceptance of the implant by the host tissue.

3) Scaffold properties

Scaffolds must present adequate properties in accordance with the future host environment. The main properties of these artificial matrices are described below. The choice of the material depends on the desired outcome.

- Mechanical properties: scaffolds should present proper mechanical resistance to support the *in vivo* stresses and should be mechanically compatible with the surrounding tissues (5).

- Porosity: the size and interconnectivity of the pores are determinant for a good cellular response. Cells have to invade and proliferate inside the scaffold and the porosity has a huge impact on nutrient diffusion, cell differentiation and tissue ingrowth (7).

- Degradation: Scaffold degradation is a fundamental property as the scaffold serves as a temporary template for tissue regeneration. The degradation must occur at a rate compatible with the new tissue formation. Moreover, the degradation process should not release toxic elements inside the body to not induce a hostile inflammatory response.

4) Polymer nanofibers

Systems with polymers scaffolds were used during the last decades. Because of their very interesting biodegradability and biocompatibility properties, polymers are the main components of tissue engineered scaffolds.

They can be classified as natural-based materials (chitosan, alginate, hyaluronic acid, collagen, etc.) and synthetic polymers. PCL (poly(ε_caprolactone), PLA (poly(lactic acid)) , PGA (poly(glycolic acid)) and PHB (poly (hydroxyl butyrate)) are the main artificial polymers that are used for synthetic polymer scaffolds (8).

Synthetic polymers have relatively good mechanical strength and their shape and degradation rate can be easily modified. However, they have hydrophobic surfaces, and unless the natural-based polymers they do not have a potential advantages for cell-recognition signals.

PGA and PLA and their co polymers (PLGA) are widely used in tissue engineering. They demonstrated good biocompatible properties. PLGA is degraded by hydrolysis through ester bonds, releasing non-toxic elements (carbon dioxide and water) at a controllable rate *in vivo*. For PLGA 50/50, the average degradation rate was estimated around 3-6 months according to (3). This time may fit with the regeneration of the periodontal tissues. That is why PLGA is often considered as a suitable material for tooth tissue engineering applications.

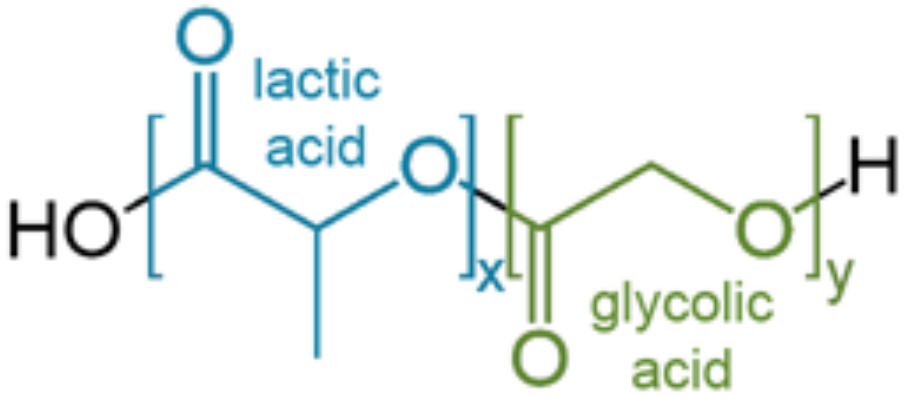

Figure 3- Poly(lactic-co-glycolic acid) structure

Nanofibers of PLGA, produced by electrospinning or jet spraying, are artificial structures capable of supporting three-dimensional tissue formation, allowing cell attachment and migration. The high porosity of these synthetic scaffolds is necessary to facilitate cell seeding and diffusion throughout the whole structure of both cells and nutrients (3). Such matrices will provide a high porous framework and reproduce the nanofibrillar component of the natural ECM (collagen structures in bones).

IV - Nanofibers synthesis techniques

Nanofibers were widely studied the last few years. There are a few different synthesis techniques to create small polymer filament with diameters smaller than 1000 nm. We described here two techniques, electrospinning and jet spraying used to create polymer fibers.

1) Electrospinning

Electrospinning allows the formation of different polymer nanofibers electrostatic interactions in order to project polymer filaments onto a ground metal screen.

Principle

A syringe is filled with a polymer source (polymer solution or melt for a constant polymer flow). An important voltage difference is applied between two electrodes placed respectively at the syringe nozzle (spinning solution) and the metal collector. It creates an electrically charged jet of polymer solution out of the nozzle. The charge localized on the surface of the solution causes a force directly opposite to the surface tension. Then the hemispherical surface of the fluid at the tip of the capillary tube elongates to form a conical shape (Taylor's cone). A critical value of the electric field could produce a repulsive force enough to overcome the surface tension and eject the charged jet. The solution jet evaporates before reaching the collector and a polymer filament is collected on the grid.

The metallic collector could be replaced by a rotating mandrel in order to orientate the fiber. Selecting an adequate high rotating speed, it is possible to obtain fiber alignment.

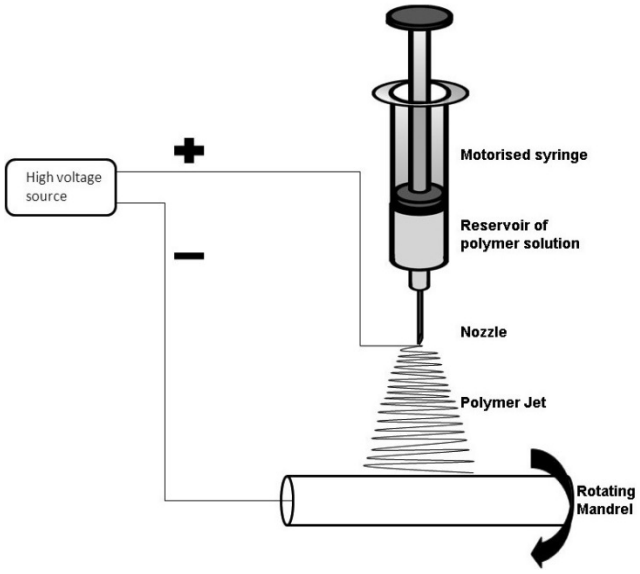

Figure 4– Electrospinning device with rotating mandrel system (9)

More than fifty different polymers have been successfully electrospun into ultra-fine fibers with a diameters ranging from a few nanometres to over 1 µm. Most of the polymers are dissolved into solvents to create a spinning polymer solution.

Quality of the produced fibers (i.e. surface roughness and dimensions) strongly depends on a set of parameters. These parameters include the solution properties (viscosity, elasticity, surface tension, and electrical conductivity), the electric field, the distance between the two electrodes and ambient parameters (temperature, humidity…) (10).

2) Jet spraying

Jet spraying is a simple and novel method for polymer nanofibers fabrication (11). With the help of an airflow, polymers are sprayed onto a target creating elongated nanofibers. The principle of Jet spraying technique is summarized in the **figure 5**. The polymer is first dissolved with an appropriate solvent. The liquid mixture, so called

polymer solution, is then attracted at the extremity of a nozzle by the air depression induced by the main air stream. A small amount of the polymer solution comes out the needle and is projected onto the collector, a Teflon grid that allows air to pass without damaging the deposited polymer fibers. The solvent, initially present in the polymer solution, is evaporated during the projection in such a way that only polymer is collected on the grid. The target could be also a rotating mandrel device as previously described with electrospinning in order to obtain aligned fibers.

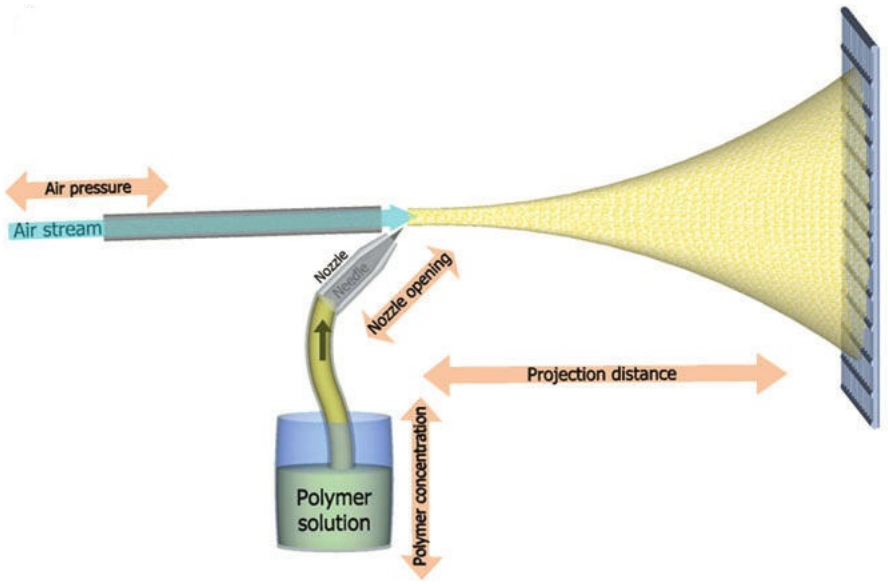

Figure 5- Jet spraying technique (11)

As with electrospinning technique, several parameters should be adjusted in order to optimize the quality of fiber production. Here we have to play with 4 main parameters: initial air pressure which drags away the polymer solution, the nozzle opening which controls the polymer solution flow, projection distance (calculated to evaporate all the residual solvent) and polymer concentration (directly related to the viscosity of the polymer solution). Solvent with high vapour pressure is needed in order to be fully evaporated during the projection of the polymer solution. We used generally for electrospinning techniques Dichloromethane (DCM). (12)

Jet spraying technique will allow the production of nanofibers with diameters ranging from 300nm to 1500nm. The nanofibers scaffolds produced with this technique present a high porosity (until 90% for polycaprolactone (PCL) nanofibers (11)).

Jet Sprayed scaffold are good candidates for regeneration scaffold because of their promising cellular interactions. Whereas cells just proliferate on the surface of the electrospun nanofibers due to their elevated density (13), they can easily migrate inside the jet-sprayed scaffolds thanks to their high porosity. In Sohier *et al.* paper, stromal cells invasion and proliferation were indeed observed onto PCL nanofibrous scaffolds (14). Human Bone Marrow Cells (hBMC) could infiltrate and colonize Jet-Sprayed nanofibers, confirming their suitable application as synthetic External Cellular Matrix (ECM) and proving their value for tissue engineering.

In comparison with electrospinning, Jet spraying offers a simple method using only an air flow to produce polymer filaments (no needs of a high voltage) where it could be more facile to incorporate external materials such as ceramic fillers.

However, because of electrospinning is an older and more studied technique, it allows to synthesize cleaner nanofibers without defects (beads) and with a correct alignment of the fibers.

V - Mineralization

1) A natural process

Bio mineralization is the process by which living organisms secrete inorganic minerals in the form of skeletons, shells, teeth, etc. It is a natural process involved during the development of these hard tissues. Bone mineralization depends on the phosphatase level through matrix vesicles (15). The supersaturation of physiological fluids in phosphate and calcium ions and others minor species (Na^+ and K^+) provokes the precipitation and

nucleation of the mineral phase as nano-sized plate-shaped particles, which are initially confined to the hole zones, and progressively extend along the collagen fibrils (16). Dimension of the minerals are ranging from 30–50 nm long, 15–30 nm wide, and 2–10 nm thick and are preferentially orientated along the fibrils.

Mineralization takes place in a confined reaction environment constructed by biomolecules- mainly polymers. Collagen, in the example of bone, builds a scaffold for the mineralization sites (17). The role of these scaffolds is to control the nucleation and growth of inorganic compounds. It is well the case in teeth and cementum, to promote the growth of hydroxyapatite with a good orientation and composition.

As inspiration from natural mechanisms of mineralization, when a tissue is damaged and a scaffold is implanted into the site, mineralization should be improved and driven by the scaffold in order to provide good mineral reconstruction. The nucleation, growth and orientation are influenced by a lot factor such as pH, composition of the surrounding medium…

Mineralization is often associated with the formation of calcium phosphate (CaP) minerals. There are many different types of calcium and phosphate minerals compositions depending on the type of hard tissue we are dealing with (see table of calcium phosphates) (18). In general, amorphous calcium phosphate, calcium deficient phosphate minerals and hydroxyapatite (HA) ($Ca_{10}(PO_4)_6(OH)_2$) are the main inorganic precipitates involving in bio-mineralization.

Table 1 – Calcium phosphate minerals

Name	Short-name	Chemical Formula
Monocalcium Phosphate Monohydrate	MCPM	$Ca(H_2PO_4)_2 \times H_2O$
Dicalcium Phosphate Dihydrate	DCPD	$CaHPO_4 \times 2H_2O$
Dicalcium Phosphate Anhydrous	DCPA	$CaHPO_4$
Octacalcium Phosphate	OCP	$Ca_8H_2(PO_4)_6 \times 5H_2O$
Amorphous Calcium Phosphate	ACP	$Ca_3(PO_4)_2$
α-Tricalcium Phosphate	α-TCP	α-$Ca_3(PO_4)_2$
β-TriCalcium Phosphate	β-TCP	β-$Ca_3(PO_4)_2$
Hydroxyapatite	HAp	$Ca_{10}(PO_4)_6(OH)_2$
TetraCalcium Phosphate	TTCP	$Ca_4(PO_4)_2O$

2) Simulated Body Fluid

A simulated body Fluid (SBF) (19) is a solution containing dissolved salts found in human blood plasma. The solution tends to be as close as possible to this physiological fluid, in terms of pH, temperature and salts concentration. **Table 2** enumerates the main ions components of the human blood plasma (19).

Table 2 – Ionic composition of human blood plasma, SBFx1 & SBFx5

Ion	Ion concentrations (mM)		
	Blood plasma	SBFx1	SBFx5
Na^+	142.0	142.0	710
K^+	5.0	5.0	25
Mg^{2+}	1.5	1.5	7.5
Ca^{2+}	2.5	2.5	12.5
Cl^-	103.0	147.8	739
HCO_3^-	27.0	4.2	21
HPO_4^{2-}	1.0	1.0	5
SO_4^2	0.5	0.5	2.5
pH	7.2-7.4	7.4	6.4

Experiments and tests using SBF were largely performed 20 years ago in tissue engineering; especially to mimic the behaviour of *in vivo* bio-mineralization (20). A similar process of mineral deposition can be simulated when samples are immersed inside a SBF solution. SBF mineralization tests, to show the bioactivity of a scaffold (future implant), were developed in several regenerative science studies.

After a specific immersion time, quality of deposited minerals (mainly calcium phosphate minerals) is analysed providing interesting comparative data about bioactivity. As previously described, mineralization is a natural and fundamental process occurring when an external material is implanted inside a hard tissue site. By mimicking the *in vivo* environment with SBF solution, bioactivity abilities can be easily estimated. Fang Yang et al. (21) and S. G. Caridade et al. (22) observed the deposition of CaP minerals onto their composite polymer matrices, showing bioactivity properties of their materials.

In order to accelerate the mineralization process, several researchers increased the global concentration of salts inside the solution. Xiaoyan Yuan et al. synthesized a 1.5 x concentrated SBF solution to control the formation of bone-like apatite on poly(L-lactic acid) fibers (23). More concentrated SBF solutions (times 5 and 10), called supersaturated SBF were synthesized again to have a faster mineralization. Consequently, average

immersion delays were shorten to a few hours for SBFx10 (24) to a few days for less concentrated SBF solution (SBFx1 or SBFx1.5) (25).

Table 3 summarizes *in vitro* mineralization assays of polymers by SBF present in the literature.

Table 3 – SBF mineralization assays on various polymers

Title	Polymer fiber substrate	Experimental details	Main achievements
Development of an electrospun nano-apatite/PCL composite membrane for GTR/GBR application (26)	Composite fibrous membranes based on nano-apatite and poly (e-caprolactone) (PCL)	SBFx1 2 & 4 weeks of immersion Kokubo conditions	the presence of nAp enhanced the bioactive behavior of the membranes
Culturing Primary Human Osteoblasts on Electrospun Poly(lactic-coglycolic acid) and Poly(lactic-co-glycolic acid)/Nanohydroxyapatite Scaffolds for Bone Tissue Engineering (27)	PLGA scaffolds	SBFx1 21 days of immersion Kokubo conditions	Embedded nano-HA can significantly enhance the formation of the bone-like apatites.
Bioactivity and Viscoelastic Characterization of Chitosan/Bioglass Composite Membranes (22)	Composite membrane of Chitosan and bioglass	SBFx1 1, 5 & 7 days of immersion Kokubo conditions	CTS/BG membrane showed improved mechanical properties and excellent apatite forming ability compared to pure CTS membrane
Preparation and bioactive properties of novel bone-repair bionanocomposites based on hydroxyapatite and bioactive glass nanoparticles (28)	Nanoparticles of hydroxyapatite introduced in porous alginate	SBFx1 7 days of immersion Kokubo conditions	Accelerated process of crystallization and growth of the apatite phase on the composite scaffold surfaces. Nanoparticles also improve the mechanical properties and stability in SBF of the polymer scaffold matrix.

Accelerated Bonelike Apatite Growth on Porous Polymer/Ceramic Composite Scaffolds in Vitro (29)	Porous PLGA/Hydroxyapatite composite scaffold	SBFx1/SBFx5 up to 5 days of immersion pH=6.4	Apatite growth on porous (PLGA/ HA) composite scaffolds was significantly faster than on porous PLGA scaffolds. Apatite coating more uniform on PLGA/HA scaffolds than on PLGA scaffolds.
Mineralization of hydroxyapatite in electrospun nanofibrous poly(L-lactic acid) scaffolds (30)	PLLA nanofibrous scaffold	SBFx1 0 to 28 days of immersion almost Kokubo conditions	Deposited mineral phase was a carbonated apatite with thin flake-like nanostructures.
A composite of Hydroxyapatite with Electrospun Biodegradable Nanofibers as a Tissue Engineering Material (31)	Nanofibrous film of PHBV	SBFx1.5 one week pH=7.25 at 36.5°C	After Hap deposition, composite surfaces became extremely hydrophilic.
Robocasting nanocomposite scaffolds of poly(caprolactone)/ hydroxyapatite incorporating modified carbon nanotubes for hard tissue reconstruction (25)	Nanofibrous scaffolds of PCL/Hydroxyapatite	SBFx1.5 1 to 14 days of immersion pH = 7.25 at 37°C	Incorporation of ionically modified carbon nanotubes into PCL-HA composition significantly improved the compressive strength and elastic modulus of the scaffolds
Formation of bone-like apatite on poly(lactid acid) fibers by a biomimetic process (23)	PLLA fibers	SBFx1.5 5 to 20 days of immersion pH = 7.3 at 37°C	After 15 days of incubation in SBF, an apatite layer (5–6 mm thickness) formed on the fibers surface.
Mechanical Properties of (poly(L-lactide-co-glycolide))- Based Fibers Coated with	PLGA fibers	SBFx3 5, 10 & 15 days of immersion pH= 7.28 at 37°C	Continuous HAp layer formed in SBF on the nanoHAp modified polymer

Hydroxyapatite Layer (32)			fibers. The tensile modulus of the fibers with a continuous layer was found to increase with the apatite layer thickness, whereas the tensile strength decreases.
Preparation of biomimetic hydroxyapatite by biomineralization and calcination using poly(L-lactide)/gelatin composite fibrous mat as template (33)	PLLA/Gelatin composite fibrous matrixes	SBFx5 24h of immersion pH=6.4	Flaky-like minerals depositing on fiber surface.
Biomineralization of electrospun poly(l-lactic acid)/gelatin composite fibrous scaffold by using a supersaturated simulated body fluid with continuous CO2 bubbling (34)	PLLA/Gelatin composite fibers	SBFx5 24h of immersion pH=6.4	Heterogenenous nucleation occurred dominantly and thermodynamical unstable brushites (dicalcium phosphate dihydrate, DCPD).
Poly(lactide-co-glycolide)/hydroxyapatite composite scaffolds for bone tissue engineering (35)	PLGA/ nano-hydroxyapatite composite scaffold	SBFx5 14 days of immersion pH=6.8 at 37 °C	Stronger biomineralization ability for PLGA/HA scaffolds than the control PLGA ones.
The synergistic effect of a hybrid graphene oxide–chitosan system and biomimetic mineralization on osteoblast functions (36)	Graphene oxide and chitosan	SBFx5 21 days of immersion pH=7.25 37°C	The combination of the chitosan–graphene oxide conjugate and biomineralization is beneficial in favorably modulating cellular activity.
Biomimetic calcium phosphate coating on electrospun poly (-caprolactone)	PCL scaffold	SBFx10 2 - 6 h of immersion pH=6.5	After 6 h, the PCL scaffolds (SBF10 6h) were fully covered with CaP

scaffolds for bone tissue engineering (37)			coating and the porous structure was lost.
Strong and tough mineralized PLGA nanofibers for tendon-to-bone scaffolds (38)	PLGA nanofibers	SBFx10 5-30min of immersion	The high toughness of this material system could be maintained without compromising on the strength with the addition of hydroxyapatite mineral.
Nanofiber Scaffolds with Gradations in Mineral Content for Mimicking the Tendon-to-Bone Insertion Site (39)	PLGA/PCL nanofibers	SBFx10 2-6h of immersion	Linear gradient in calcium phosphate content achieved across the surface of the nanofiber mat.
Advanced tissue engineering scaffold design for regeneration of the complex hierarchical periodontal structure (40)	Biphasic PLC scaffold	SBFx10 30 min pH=7, 37 °C	Alkaline phosphatase activity and mineralization was significantly increased in the CaP-coated samples.

3) Polymer nanocomposite

A third way to initiate the mineralization of a new polymeric scaffold is to incorporate calcium phosphate particles during its synthesis. Hydroxyapatite can be easily introduced by several methods to PLGA, PCL nanofibers. **Table 4** lists the different assays on the fabrication of polymer and hydroxyapatite composites. A commonly used technique to produce nanocomposite of polymer and hydroxyapatite is electrospinning. Nanoparticles are first mixed to the polymer solution. The new blend, stirred energetically, contains the polymer solution with HA nanoparticles in suspension. The mixture is then inserted into a syringe and projected onto a collector to produce composite nanofibers as shown on **figure 4**. Authors listed in **table 4** used hydroxyapatite

nanoparticles with dimensions often smaller than 200nm. Amorphous Calcium phosphate and tri-Calcium Phosphate were sometimes also incorporated to PDLLA (41) and PCL (42).

The percentage in mass of CaP nanoparticles is comprised between 0 and 50% wt. Viscosity of the polymer solution changed with the amount of fillers. Thus it has some consequences on the quality and the synthesis parameters of the electrospinning device.

With this technique, nanoparticles are incorporated inside the fibers as shown on the TEM image (**figure 6**) (21). The HA crystals are well located inside the fiber and do not appear at the surface unless if the amount of fillers is too high.

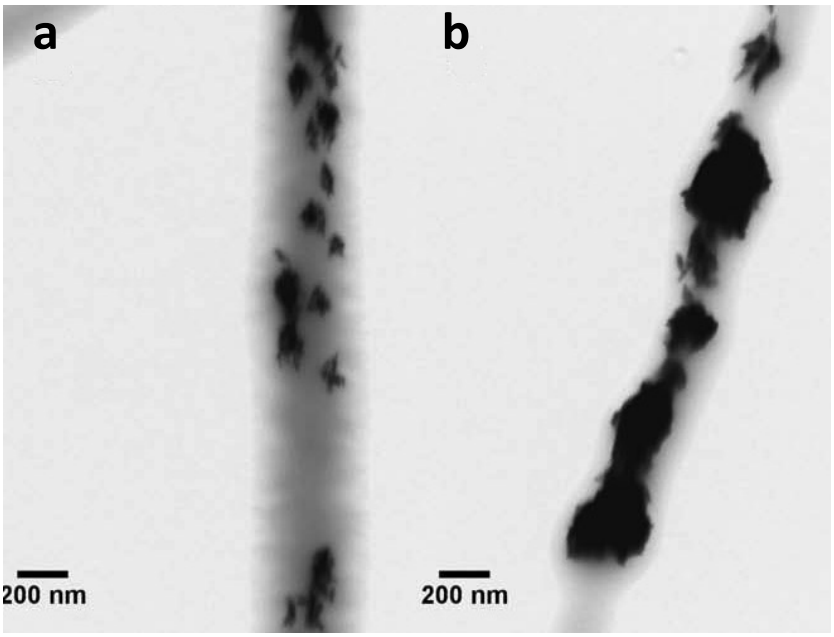

Figure 6- Transmission electron micrograph of HA nanoparticles incorporated inside electrospun PCL fibers (26)

Table 4 – Polymer/hydroxyapatite nano-composites fabrication present in the literature

Title	Experimental details	Main achievements
Poly(lactide-co-glycolide)/hydroxyapatite nanofibrous scaffolds fabricated by electrospinning for bone tissue engineering (7) (43)	Electrospinning mixture suspension PLGA+ HA particles (266.6+/- 7.3 nm) 0 to 15 % wt of HA particles in the polymer blend	Good mineralization at the surface of the fibers. %wt HA should be higher than 5 to have an homogeneous mineral coating. In vitro mineralization in a 5x simulated body fluid (SBF) revealed that the PLGA/HAp nanofibrous scaffolds had stronger biomineralization ability than the control PLGA scaffolds.
Culturing Primary Human Osteoblasts on Electrospun Poly(lactic-coglycolic acid) and Poly(lactic-co-glycolic acid)/Nanohydroxyapatite Scaffolds for Bone Tissue Engineering (27)	Electrospinning PLGA + nano HA particles (205nm x 33nm) 30%wt of HA paticles in the blend	Embedded nano-HA can significantly enhance the formation of the bone-like apatites
Control of Osteogenic Differentiation and Mineralization of Human Mesenchymal Stem Cells on Composite Nanofibers Containing Poly[lactic-co-(glycolic acid)] and Hydroxyapatite (44)	Electrospinning PLGA + HA nanoparticles (< 200nm) 20 & 40%wt of HA particles	Reasonable mineralization with 0.4 % of HA HA homogeneously dispersed in the nanofibers, and the roughness increased along with the amount of incorporated HA.
Aligned PLGA/HA nanofibrous nanocomposite scaffolds for bone tissue engineering (45)	Electrospinning PLGA + HA nanoparticles (100-150 nm) 1, 5, 10 and 20 wt.%	Addition of different amounts of nano-HA increased the average fiber diameter from 300 nm (neat PLGA) to 700 nm (20% nano-HA) Agglomeration of HA at higher HA concentration (>10%)

The influence of electrospun fiber scaffold orientation and nano-hydroxyapatite content on the development of tooth bud stem cell in vitro (46)	Electrospinning PLGA+HA 33 and 50%wt	PLGA/HA scaffolds fabricated with preferential alignment. nHAs have an effect on cell proliferation.
Poly(lactide-co-glycolide)/hydroxyapatite composite scaffolds for bone tissue engineering (35)	Gas forming and particulate leaching (GF/PL) method PLGA + HA nanoparticles (100nm) 50%	Novel method for fabricating a polymer/nano-bioceramic composite scaffold (PLGA/HA) with high exposure of the bioceramics to the scaffold surface.
Development of an electrospun nano-apatite/PCL composite membraneGTR/GBR application (26)	Electrospinning PCL + HA nanoparticles (rod like shape 20nm*60nm) 25 and 50 %wt	PCL/HA nanofiber diamters ranging from 320nm to 430nm NPs incorporated inside the fibers
Functionally graded electrospun polycaprolactone and b-tricalcium phosphate nanocomposites for tissue engineering applications (42)	hybrid twin-screw extrusion/electrospinning (TSEE) PCL +βTri Calcium Phosphate (βTCP) (50 nm -2.5 µm) gradient of NPs contents from 0 to 15 wt%	Concentration of tricalcium phosphate nanoparticles tailored to vary in a targeted/ controlled manner between the two surfaces of the scaffold mesh
Electrospun biomimetic nanocomposite nanofibers of hydroxyapatite/chitosan for bone tissue engineering (47)	Electrospinning Chitosan + HA nanoparticles (100 nm* 30 nm) 30%wt	HAp nanoparticles with some aggregations were incorporated into the electrospun nanofibers. HAp/CTS nanofibers with a diameters of 214 +- 25 nm
Amorphous calcium phosphate/poly(D,L-lactic acid) composite nanofibers: Electrospinning preparation and biomineralization (41)	Electrospinning PDLLA/Amorphous Calcium Phosphate nanoparticles (20-80 nm) No information	Different architectures including the nanofibrous mesh and tube consisting of ACP/PDLLA composite nanofibers were obtained.

Poly-L-lactic acid/hydroapatite hybrid membrane for bone tissue regeneration (48)	Electrospinning PLLA/HA nanoparticles (40-70nm * 15 nm) No information	Very good mechanical and characterization assays on the fibers. Interesting comparison between the two matrices (PLLA without and with HA) SEM/XRD/IR/EDX/DSC/Tensile stress/Degradation test/Osteoblast cell cultures
Nanofibrous Poly(lactic acid)/hydroxyapatite composite scaffolds for guided tissue regeneration (49)	Electrospinning PLA +HA nanoparticles (35 nm) 5 and 20%wt	Mixture of PLA and HA formed smooth nanofibers without lumps. incorporation of HA increased the mechanical strength of the nanofibers and changed the morphology, increasing the mean fiber diameter and pore size.

VI - Objectives

The aim of this master thesis is to evaluate different techniques for the preparation and mineralization of nanofibrous PLGA matrices. We know that, in order to increase the bioactivity and the cellular response of these scaffolds, we have to initiate the mineralization before implantation. As the future implant site will be at the interface between the cementum and the jaw bone, we target a deposition of hydroxyapatite in order to mimic this hard tissue in composition and morphology. A mineral coating at the surface of PLGA nanofibers would modify the scaffold properties and could improve cell biocompatibility (invasion and proliferation).

We will discuss in this work three different potential ways of mineralization. Electrospun PLGA matrices will be mineralized by normal and supersaturated SBF solutions. Then, jet spraying technique will allow the fabrication of porous PLGA/HA nanocomposite by making a polymer solution with HA nanoparticles in suspension. The last technique consists of a co-projection of a polymer solution and a suspension of nHA

in water with the jet spraying device. The mineralized matrices will be compared and features of the obtained scaffolds will be discussed.

VII - Material and methods

1) Mineralization

We decided to go through three different approaches in order to incorporate Calcium Phosphate minerals inside PLGA nanofiber matrices. The first one consists to precipitate CaP crystals onto a NaOH activated surface of electrospun PLGA matrices by soaking them into a high concentrated salt solution. The two others use Jet spraying technique to create a nano-composite of hydroxyapatite (HA) and PLGA, mixing or co-projecting the two materials.

2) Simulated Body Fluid Mineralization

A promising way to promote periodontal tissues regeneration is to initiate mineralization of the scaffold before implantation. In this section, we explored a mineralization process with SBF solutions to build a calcium phosphate mineral layer on the surface of PLGA fibers produced by electrospinning.

a) Electrospinning parameters

PLGA nanofibers were produced through electrospinning. The polymer, poly(lactic-co-glycolic acid (PLGA) with a molar ratio of 50:50 (Mn 30,000-60,000; inherent viscosity 0.55-0.75 dL/g, Sigma-Aldrich), was dissolved into dichloromethane (DCM) solution. Concentration of PLGA into the solvent was 0.33g/mL.

The electrospinning device (**figure 7**) contains a rotating mandrel situated in the middle of two syringes. The mandrel collects the filaments simultaneously produced by the two polymer reservoirs. A voltage difference of 24V is applied between the two electrodes (located at the syringes) with a polymer flow of 6mL/h. The distance between the target and the electrodes is 10 cm.

Electrospun nanofibers are then stored in Petri dish and put inside a desiccator in order to prevent the degradation of the polymer before further characterization tests.

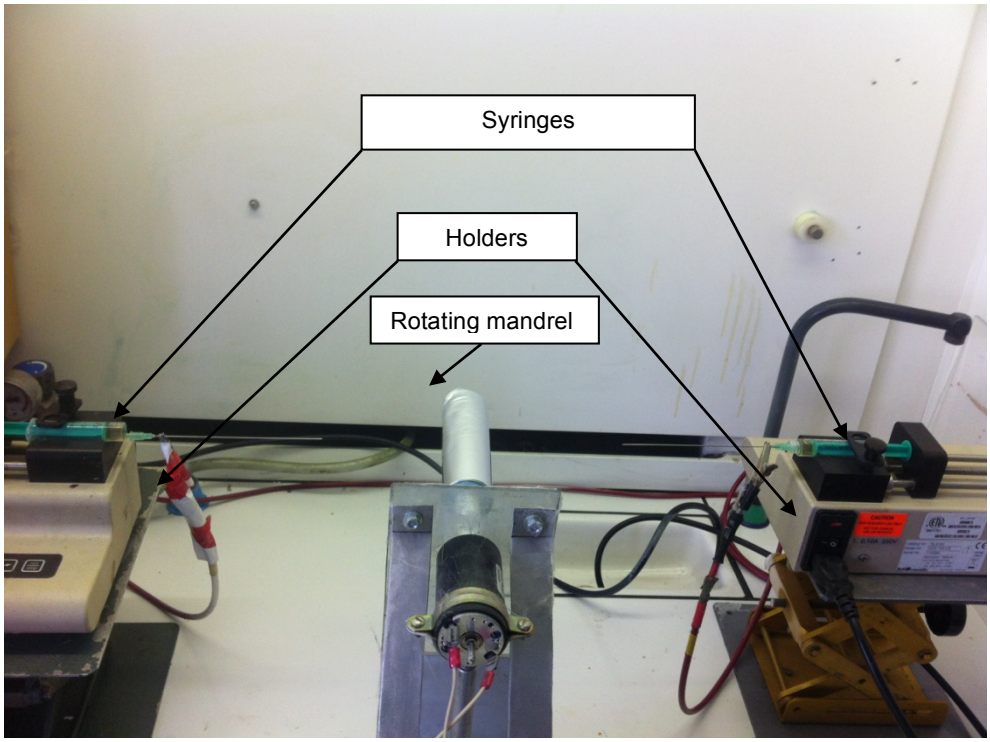

Figure 7 – Dual extrusion electrospinning with a rotating mandrel diagram.

Figure 8 represents one of the PLGA matrices fabricated under the previous conditions at two different magnifications. Fibers diameter range is between 600nm and 700nm. A global alignment of the PLGA fibers could be observed on the **figures 8-A & B**.

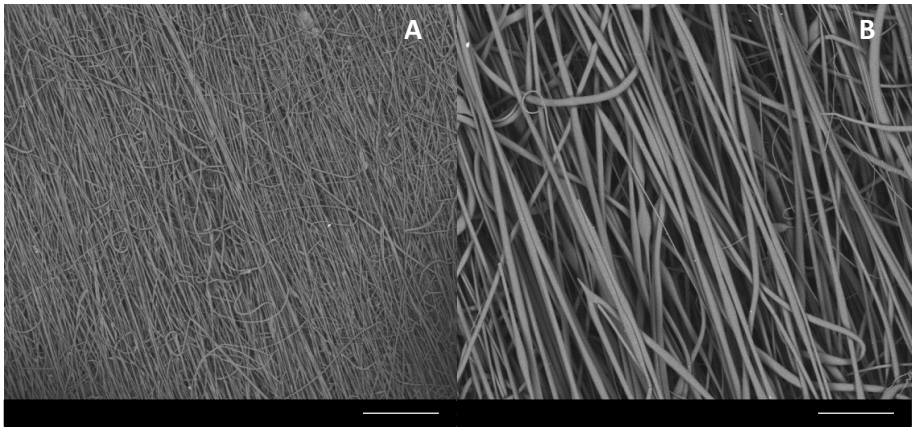

Figure 8 - Aligned nanofibers of PLGA produced by electrospinning (magnification A: x50 and B: x300/bare scales: 500µm (A)/ 100µm (B))

b) SBF preparation

We prepared two types of Simulated Body Fluids: a normal SBF solution (SBFx1) and a 5 times more concentrated one (SBFx5).

Kokubo and al. (20) described carefully the main steps of SBF synthesis and some crucial precautions. Indeed, because of the high proportion of salts that should be completely dissolved, SBF is a very unstable solution. **Table 5** lists the different salt products and their quantity needed to prepare one liter of SBF solution. The solution should remain till the end of the synthesis entirely transparent. Precipitation has to be avoided during the synthesis to preserve properties similar to blood fluid.

Prepare a suitable SBF solution is difficult because many parameters are involved in its stability such as pH, temperature, stirring, quality of the recipient (presence of scratch on the beaker), etc. All these factors can initiate and induce a sudden salt precipitation in the beaker.

A protocol in **annex 1** describes the synthesis process that we performed to produce SBF solutions. It follows the Kokubo's protocol written in his paper (19) for the solution SBFx1.

However, we had to adapt some parts for the more concentrated SBFx5. Kokubo worked in his study cases only with low concentrated SBF solutions (SBFx1 or 1.5).

A low pH has to be reached (between 1 & 2) in order to correctly dissolve calcium chloride and sodium sulphate salts. After the complete dissolution of these two components, the global pH of the solution must be slowly increased to 7.4 with the buffering agent TRIS (**tris(hydroxymethyl)aminomethane**). During SBF x5 solution synthesis, we observed salt precipitation around a pH value of 6.5. As this critical value was overcome, the solution became blurred due to calcium phosphate or sodium chloride precipitation. We finally obtained a transparent SBFx5 solution by keeping the pH at a value of 6.4.

The prepared solutions were stored inside plastic containers and kept in a fridge at 5-10°C.

Table 5 – Order and amounts of reagents for preparing 1000 ml of SBFx1 & SBFx5

Reagent	**Formula**	**Amount SBF x1 (g)**	**SBF x5 (g)**
(1) Sodium Chloride	NaCl	8.035	40.175
(2) Sodium hydrogen carbonate	$NaHCO_3$	0.355	1.775
(3) Potassium chloride	KCl	0.225	1.125
(4) Di-potassium hydrogen phosphate trihydrate	$K_2HPO_4.3H_2O$	0.231	1.155
(5) Magnesium chloride hexahydrate	$MgCl_2.6H_2O$	0.311	1.555
(7) calcium chloride	$CaCl_2$	0.292	1.46
(8) sodium sulfate	Na_2SO_4	0.072	0.36
(9) Tris-hydroxymethyl aminomethane	$((HOCH_2)_3CNH_2)$(Tris)	6.118	30.59
		mL	
(6/10) 1M (mol/l) Hydrochloric Acid	1M-HCl	45	225
Demineralized Water	H_2O	700	3500

c) SBF immersion experiments

Figure 9 summarizes the main steps of the SBF experiments.

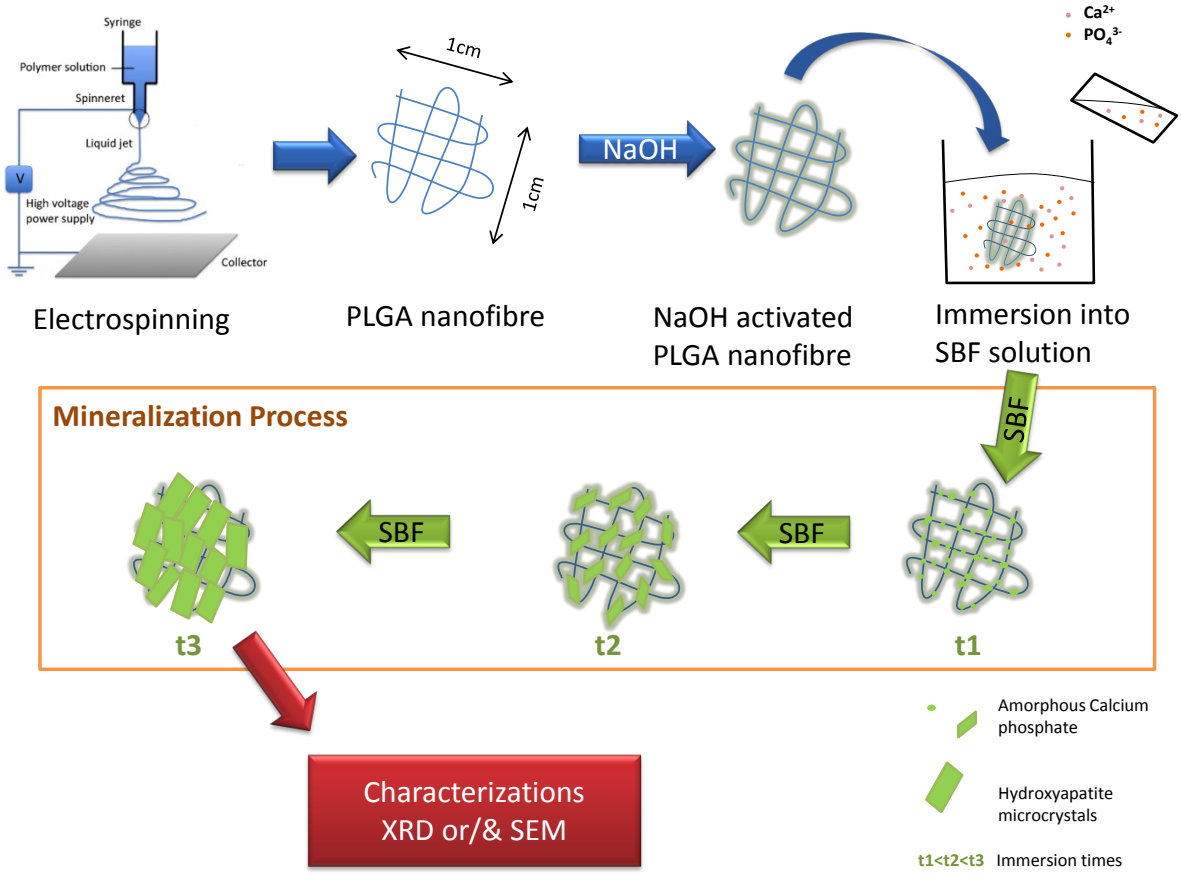

Figure 9– Schematic of Simulated Body fluid experiment steps

PLGA nanofibers fabricated by electrospinning (see **electrospinning parameters**) were cut in small squared pieces of 1cmx1cm. The new dimensioned samples were then activated by NaOH solution (0.01M). With a paintbrush, a small amount of NaOH liquid was spread on the surface of the matrices. In order to have a reproducible process, two ways with the paintbrush were performed to deposit approximately the same volume of liquid. After a specific time, samples were gently rinsed with deionized water twice.

NaOH activation on PLGA polymer allows to break chemical bonds of the PLGA polymers chains, to produce two new active sites (-COOH and -OH). The hydrolysis of the polymer liberates acid sites which in presence of NaOH (basic conditions) become negatively charged (50) (see **figure 9**). The aim of this step is to activate only the surface of the nanofibrous matrices. The new negative charges present on the surface will attract the positive ions, Calcium Ca^{2+} and initiate the process of mineralization as shown in **figure 10**.

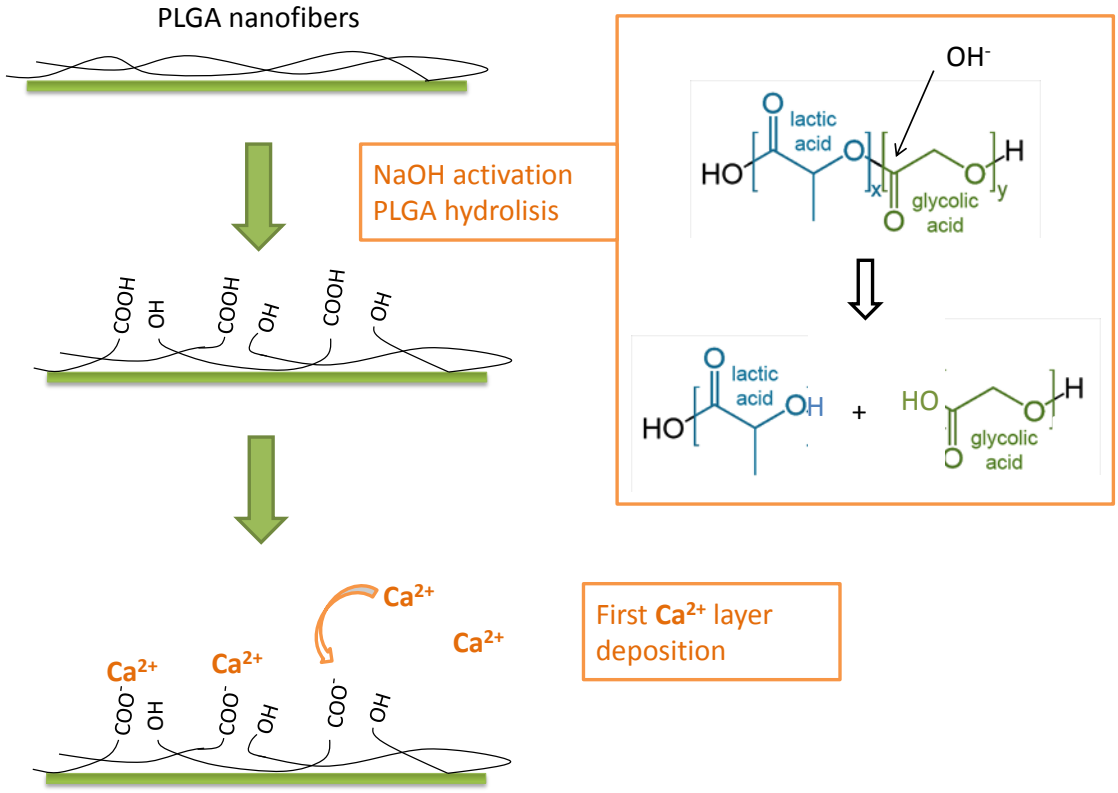

Figure 10 Hydrolysis of PLGA polymer in basic solution (NaOH)+ beginning of Ca^{2+} mineral deposition.

After NaOH activation, samples were attached to the cap of a 40mL container by welding the four corners of the PLGA matrix to the plastic cap, see **figure 11**. Plastic container was closed and returned in order to immerse the PLGA sample with SBF

solution. This system allows a good stability of the sample at the bottom of the bottle, which is hard to achieve because of the important hydrophobicity of PLGA. Samples were inserted in an incubator at a temperature of 37 °C.

After specific times of immersion, PLGA matrices were pull out and rinsed with deionized water. When the samples were completely dry, they were stored inside a desiccator waiting for further characterizations. Times of immersions were selected by comparison with the previous SBF mineralization studies described in the literature (see table 2). We settled on shorter times for SBFx5 (from 1 to 5 days) because the mineralization is supposed to be faster due to the high salt concentrations (**table 5**).

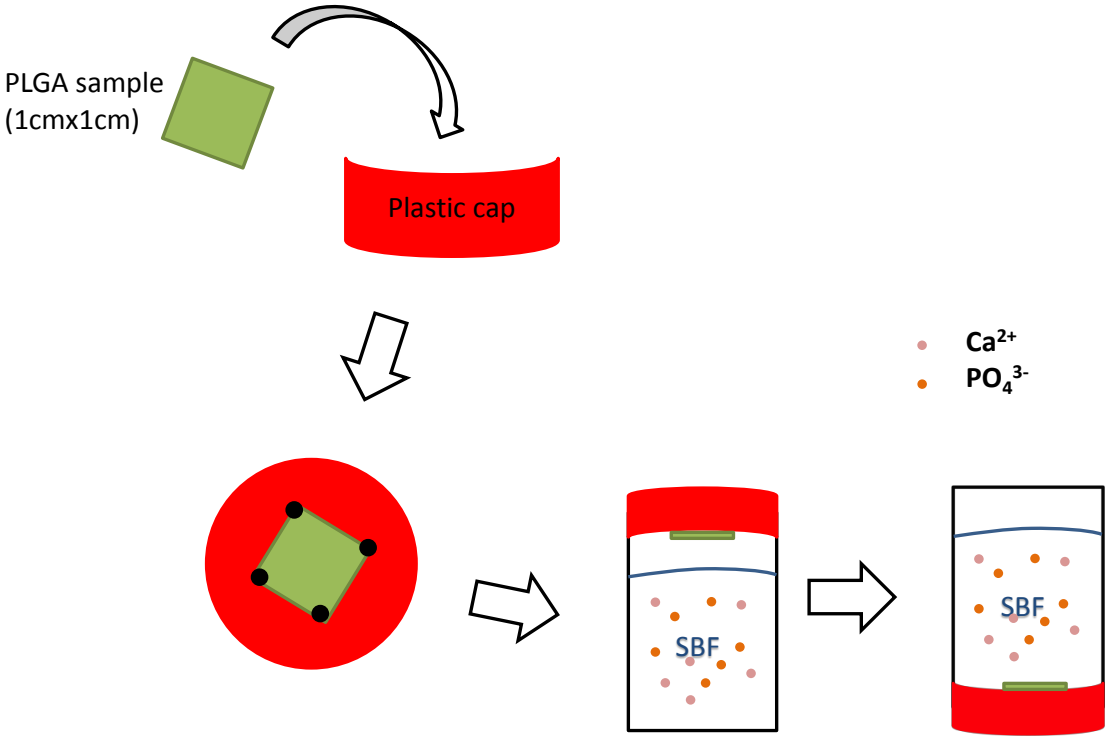

Figure 11– SBF immersion system of PLGA matrices

In order to find the more convenient and efficient method to mineralize the PLGA fibers, we tested a panel of samples changing 3 variables: SBF immersion time, concentration of the SBF solution (x1 or x5) and activation time of the surface of the sample by NaOH solution. **Table 6** the schedule of the parameters tested during the mineralization of the different samples.

Table 6 - Mineralization by SBFx1 and SBFx5 samples

<table>
<tr><td colspan="2">Immersion time in SBF (days)</td><td colspan="4">NaOH activation times</td></tr>
<tr><td>SBF x1</td><td>SBF x5</td><td rowspan="6">0s</td><td rowspan="6">30s</td><td rowspan="6">1 min</td><td rowspan="6">5 min</td></tr>
<tr><td>1</td><td>1</td></tr>
<tr><td>5</td><td>2</td></tr>
<tr><td>7</td><td>5</td></tr>
<tr><td>14</td><td></td></tr>
<tr><td>21</td><td></td></tr>
</table>

2) Jet spraying of Hydroxyapatite nanoparticles & PLGA mixture

a) Principle

Figure 12-1 summarizes the first Jet Spray technique employed to create polymer fibers containing hydroxyapatite nanoparticles.

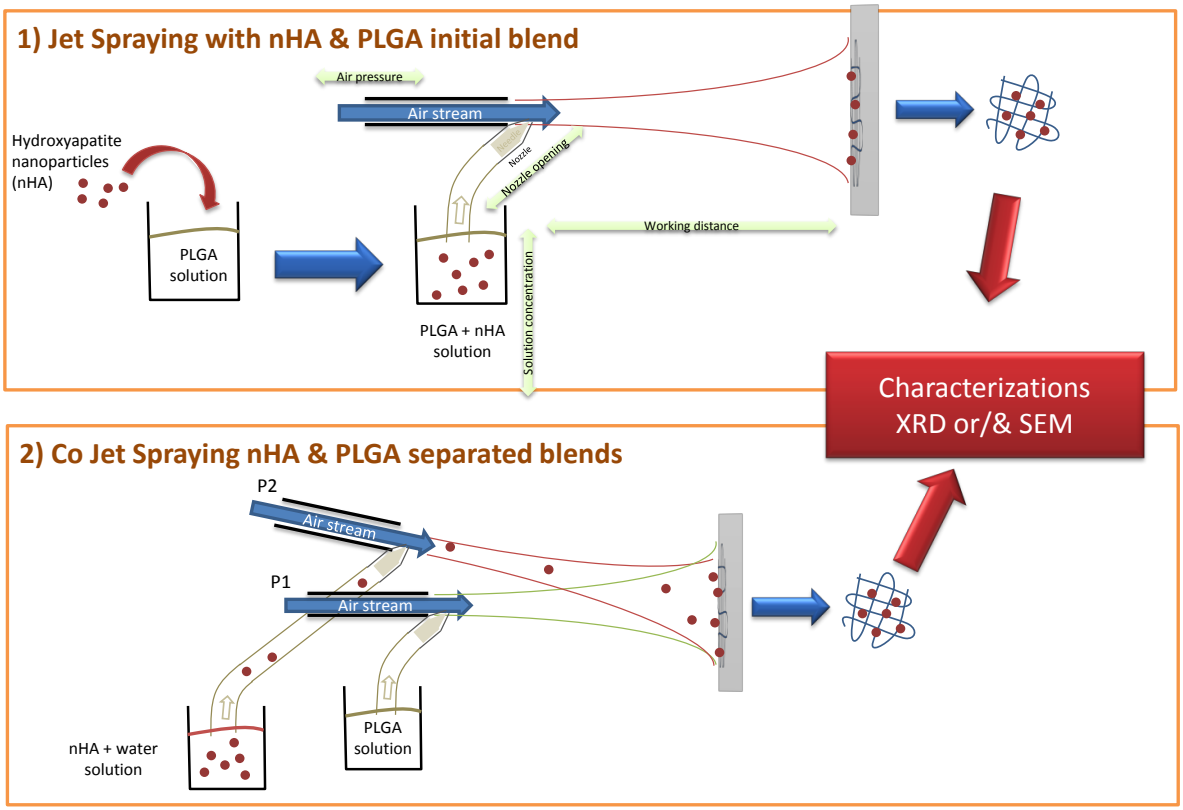

Figure 12– Mineralization processes- 1) Jet spraying with nHA and PLGA initial mixture and 2) Co Jet spraying nHA and PLGA separated blends

A precise amount of PLGA (5O/5O lactic/glycolic) was dissolved in Chloroform (0.125g of PLGA / 1mL of solvent) to create the polymer solution. Then, hydroxyapatite nanoparticles (nHA) were inserted to the previous PLGA polymer solution. The mixture was stirred during 10 minutes at 1000 rpm in order to homogenise the solution. Then, the blend was projected to the target grid to produce a nanocomposite of polymer and hydroxyapatite. The goal was to incorporate calcium phosphate minerals inside and around the PLGA fibers through this technique.

Nanoparticles of hydroxyapatite were purchased from Sigma. Their average dimensions were 200nm (BET measurement). These particles were chosen because their size and composition correlate to the initial calcium phosphate precipitates *in vivo*.

b) Experiments

We produced six PLGA matrices containing HA nanoparticles with this technique. **Table 6$7** lists the fabricated samples with their corresponding synthesis parameters. The six first samples have a nHA content varying from 5% to 30%. The 7th experiment has a concentration too high (50%) to produce convenient PLGA fibers.

Parameters of the Jet spraying machine (opening needle/ Nozzle distance/ air flow pressure and working distance) were selected thank to previous work of a Ph. D. student that established appropriate parameters to produce PLGA matrices without difficulties.

Only the PLGA/nHA composition ratio is varying between the samples, except for the 6th sample where the nozzle opening was increased to accelerate the filament formation and limit the formation of aggregates at the end of the needle. Synthesis time also varied as a consequence of the insertion of nHA, because HA nanoparticles make the polymer solution more viscous.

For the last sample 7th, even by changing the parameters (nozzle opening and air flow pressure), we were not able to extract PLGA filaments from the initial solution. We concluded that the PLGA/nHA ratio should be inferior at 0.5 to have a reasonable viscosity and not obstruct the device.

Table 7 – Parameters of JS samples

JET SPRAYING Experiments						
N° sample	Content	Opening Needle (mm)	Nozzle distance (mm)	Working distance (cm)	Air flow pressure (Bar)	Synthesis time
1	PLGA	3.8	2.5	30	6.5	6 min
2	PLGA + 5% nHA	3.8	2.5	30	6.5	7 min
3	PLGA + 15% nHA	3.8	2.5	30	6.5	7 min
4	PLGA + 25% nHA	3.8	2.5	30	6.5	28 min
5	PLGA + 30% nHA (a)	3.8	2.5	30	6.5	40 min
6	PLGA + 30% nHA (b)	4.5	2.5	30	6.5	20 min
7	PLGA + 50% nHA	x	x	x	x	x

3) Separated co-projection of nHA and PLGA

a) Principle

Figure 12-2 shows the Jet spraying method used to realize a co projection of hydroxyapatite nanoparticles and PLGA polymer. The principle is to simultaneously produce a PLGA fiber with a first spray gun (G1) and project nanoparticles with a second spray gun (G2).

Nanoparticles are incorporated to the polymer fibers during their formation. As the previous experiment, nHA should integrate the polymer and form a nano-composite with PLGA. We expected for this technique a deposition of the nanoparticles at the surface of the PLGA fibers.

b) Experiments

Nanoparticles of Hydroxyapatite were first mixed with a common solvent: distilled water (better homogeneity than with ethanol or chloroform). Water + nHA were stirred at 300 rpm during 10 minutes and with ultrasonic waves and during 5 minutes. Preliminary tests on a glass support were performed to adjust parameters of the second spray gun. Glass samples were examined with a microscope. The Combination of parameters offering the best repartition of nHA and with fewer defaults was selected. We first adopted a pressure of 10 bars for G2 with a nozzle opening of 1.3 mm. We kept the same parameters to produce the PLGA fiber with the spray gun n°1. Then, we realized 7 jet sprayed PLGA matrices varying the air flow (G2) (6.5 or 10 bars) and the concentration of the nHA inside the water (from 1 to 2 mg/mL). Parameters are listed in **table 8** for the two guns.

We first started on the production of PLGA nanofibers for several minutes to produce a non-mineralized scaffold (t1). Then we projected nanoparticles with the gun n°2 without turning off the first gun during 10 minutes (t2). Thus we obtain a composite layer of PLGA without nHA particles and PLGA fiber with. The bottom layer of PLGA was created in order to consolidate the fiber and facilitate its removal from the grid. We will analyse only the top layer later to characterize the composite.

Table 8 listed the 6 samples with their respective parameters.

Table 8 - Set of parameters for Co Jet spraying of PLGA and nHA

Co Jet spraying Gun								
N° sample		Content	Needle distance (mm)	Nozzle opening (mm)	Air flow pressure	PLGA/nHA concentration	Synthesis time (t1/t2)	Working distance (d1/d2)
1	G1	PLGA + chloroform	3.6	2.85	6.5 bar	0.1 g/mL	10 min	30 cm
	G2	nHA + water	/	1. 3	10 bar	1.85 mg/mL	10 min	38 cm
2	G1	PLGA + chloroform	3.6	2.85	6.5 bar	0.1 g/mL	27 min	30 cm
	G2	nHA + water	/	1.3	10 bar	1 mg/mL	10 min	38 cm
3	G1	PLGA + chloroform	3.6	2.85	6.5 bar	0.1 g/mL	4 min	30 cm
	G2	nHA + water	/	1. 29	10 bar	1 mg/mL	11 min	38 cm
4	G1	PLGA + chloroform	3.6	2.85	6.5 bar	0.1 g/mL	5 min	30 cm
	G2	nHA + water	/	1.39	10 bar	1 mg/mL	7 min	38 cm
5	G1	PLGA + chloroform	3.6	2.85	6.5 bar	0.1g/mL	4 min	30cm
	G2	nHA + water	/	1.35	6.5 bar	1 mg/mL	8 min	38 cm
6	G1	PLGA + chloroform	3.6	2.85	6.5 bar	0.1g/mL	4 min	30cm
	G2	nHA + water	/	1.45	6.5 bar	2 mg/mL	12 min	38 cm

The second gun has a working distance larger because of its location (see **figure 12-1**). We have to adjust carefully the direction of the second air flow to project nHA at the adequate spot, where the PLGA nanofibers are collected. A non-alignment of the two air flows could induce a poor repartition of the nanoparticles on the sample.

4) Characterization methods

Samples were characterized by two main techniques: X-ray diffraction and Scanning Electron Microscopy. Additional tests were performed on PLGA nanofibers in order to characterize their degradation.

a) X-Ray Diffraction

X-ray diffraction is versatile, non-destructive analytical technique for identification and quantitative determination of the various crystalline forms of compounds present in powdered or solid samples. It is based on the diffraction of an incident beam that interferes with atomic planes of a crystal. As the Bragg's law explained, an X-ray beam will diffract at some specific angles characteristic of the periodicity and the arrangement of the crystal.

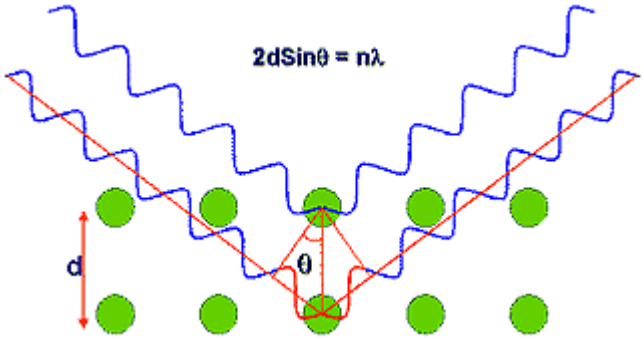

Figure 13– Bragg's law (51)

PLGA samples were analysed by X-ray diffraction. As PLGA is an amorphous polymer, X-rays will not be diffracted by the polymer. Only a small signal will be collected deforming softly the base line of the spectra. If others crystals are present, as Calcium phosphate precipitates or hydroxyapatite particles, x-rays should be diffracted and characterized peaks will appear at specific angles.

We scanned the samples with X-ray angles selected from 20 to 40° (X-ray generator/ tension= 45kV/Current=30mA).

There was no specific samples preparation to perform this technique. PLGA fibers were more or less flat (except for SBF samples), the only requirement for good diffraction measurement. If the sample presents some relief, it could slightly shift diffraction angles and widen the peaks.

b) Scanning electron microscopy

The electron microscopy technique uses an electron beam that bombards the sample in order to induce interactions with the matter. Electrons will interfere with the sample and produce several types of signals such as secondary electrons (SE), backscattered electrons (BSC) and X-rays. With electron signals, contrasted images could be obtained showing the morphology of the fibers. Phase identification is available thanks to the contrast (heavier element will appear in white). Magnifications of the images are ranging from x300 to x25000 for the more precise images.

A complementary technique, Energy dispersive X-ray spectroscopy, allows by collecting the x-ray signals emitted by the matter to identify elements present inside the sample.

In order to have a good contrast, SEM samples should be conductive. Before introducing to the SEM working chamber, a very thin film of carbon was deposited on the PLGA membrane. This step called metallization allows a free interaction between electrons and the matter.

PLGA nanofiber is a sensitive material. If the electron beam intensity is too strong, PLGA film could be damaged. SEM parameters such as gun voltage, aperture diameters and magnification should be correctly adjusted to not burn the polymer. This degradation phenomenon could sometimes limit structural observations at high magnification (> x3000).

c) Degradation assays

Degradation experiments were performed on jet sprayed PLGA samples in order to quantify the morphology evolution of the matrices inside an aqueous solution. We know that the PLGA nanofibers structures greatly vary (high shrinkage of the samples) when they are immersed inside SBF solutions. Samples of 1cm*1cm were soaked inside a physiological solution of PBS (Phosphate Buffered Saline) during 21 days at 37°C. PLGA pieces were measured before and after their immersion. PLGA in presence of water and oxygen is subjected to hydrolysis process; the structural quality of the matrices is rapidly damaged. PLGA sample sizes were significantly reduced making the dimension measurement difficult. All the values listed in the characterization results are approximate but it demonstrates well the degradation shrinkage of the PLGA fibers.

VIII - Characterization results

We first characterized our samples with X-Ray Diffraction (XRD) technique to detect the presence of mineral phases (calcium phosphate) on PLGA matrices. Because of the relative availability of the XRD device and the rapid analysis of one sample (no special preparation needed as SEM technique), this method was used in first instance. Then, where XRD indicates some crystallinity, the morphologies of the fibers and the deposited minerals of the sample were analysed through Scanning Electron Microscopy (SEM). Energy Dispersive X-ray Spectroscopy (EDX), available with SEM, provides the exact composition of the minerals on/in the PLGA fibers.

1) X-Ray Diffraction

a) Simulated Body Fluid x1

Figure 14 represents the XRD patterns of all the 20 samples mineralized by SBFx1 solutions with different immersion times: 1, 5, 7, 14 & 21 days (A, B,C, D & E) and NaOH activation: 0s, 30s, 1min and 5min (a, b, c and d).

We may observe diffracted peaks for some samples:

- One day, 0s (A-a)

- one day, 1 min (A-c)

- 7 days, 1 min (C-c)

- 21 days, 0s, 30s, 1 in and 5 min (E-a,b,c).

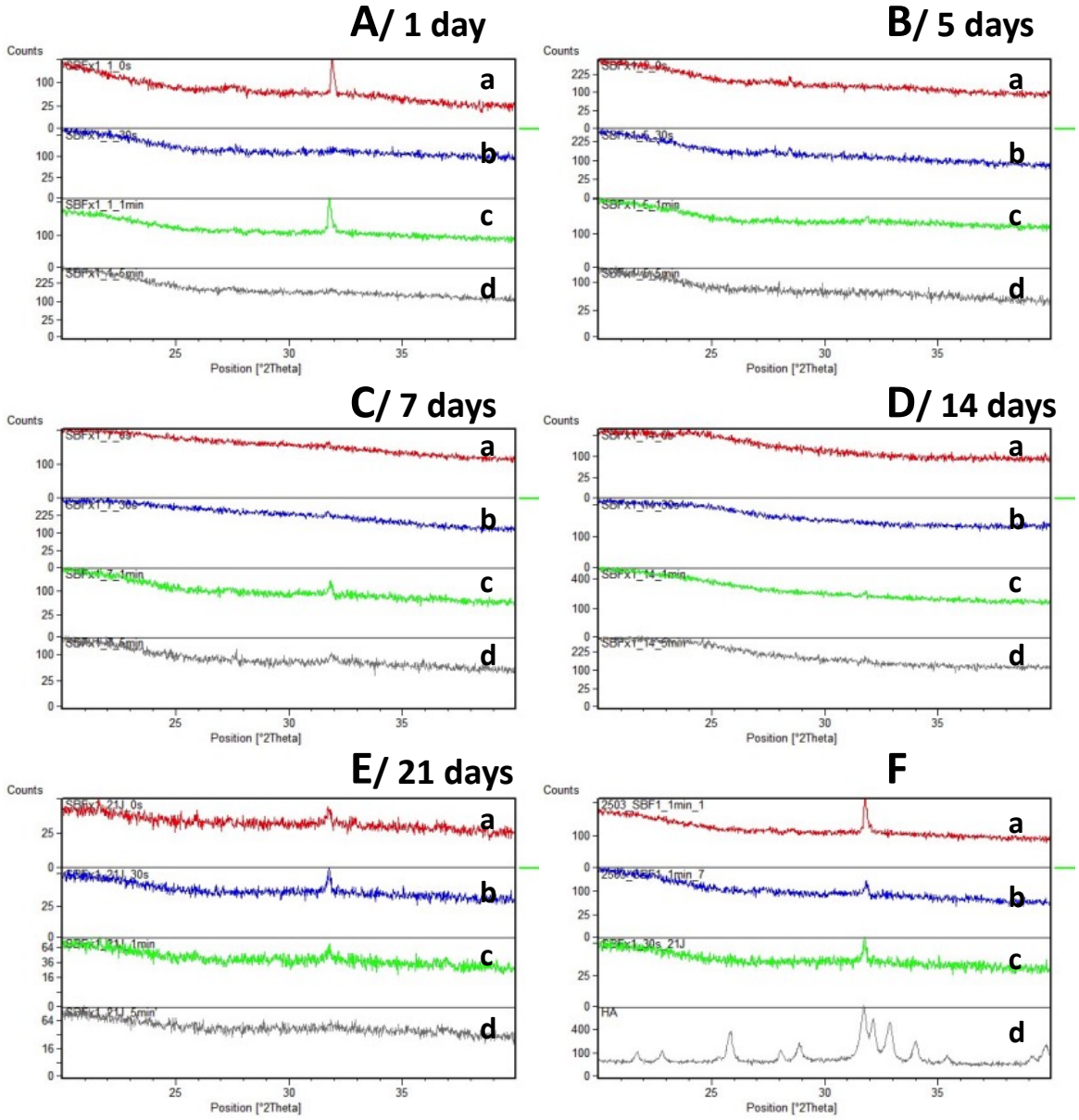

Figure 14 - XRD graphics of PLGA samples soaking during 1, 5, 7, 14 & 21 days (respectively A, B, C, D & E) with different NaOH activation: 0s, 30s, 1 min & 5 min (a,b,c & d).

F: Comparison of 3 spectra where a diffracted peak appears (a: 1day/0s, b: 1day/1min, c: 7days/1min and d: with HA NPs diffraction pattern).

On these samples, one main peak appears at 2theta = 32°. On **Figure 14-F**, 3 samples where the diffracted peak appears (i.e. SBFX1-1 day-0s/ SBFX1-1 day-1min/ SBFX1-5 day-1min) were plotted with a diffracted pattern of hydroxyapatite nanoparticles. This control provides an efficient model to compare the deposited mineral structure to pure hydroxyapatite.

PLGA matrices after 21 days of immersions were damaged by the SBF solution and the structural properties of the polymer were completely changed. As a result, it was not possible to remove the samples from the plastic cap without breakage. We were able to make XRD measurements with the remaining powder of the matrix.

b) Simulated Body Fluid x5

Figure 15 shows the XRD patterns of SBFx5 mineralized samples with immersion times of 1, 2, 3.5 and 5 days (A, B, C & D). The two first experiments with short immersion times (1 and 2 days) do not present well defined diffracted peaks. However, the samples immersed for 3.5 and 5 days show diffracted beams around 32° and 27° (figure 12-C and D).

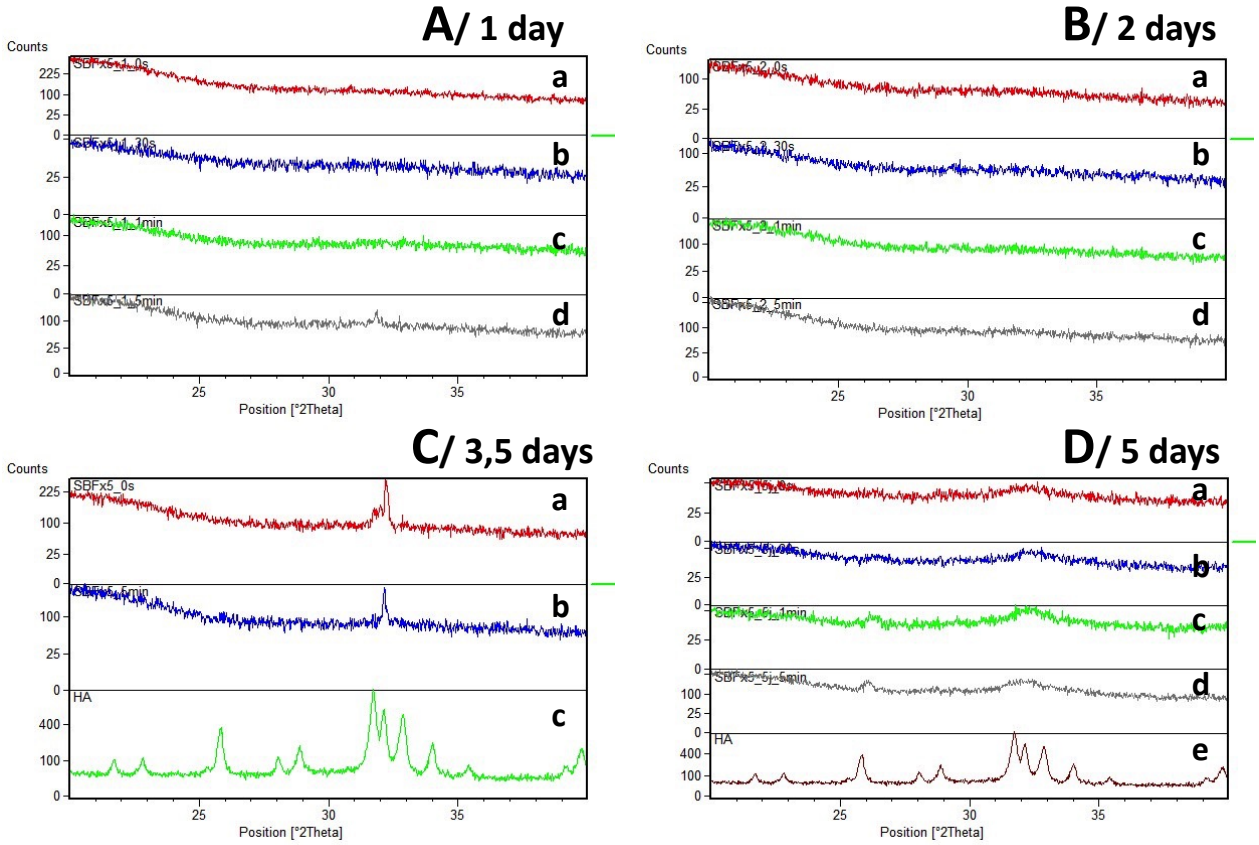

Figure 15 – XRD graphics of PLGA samples soaking during 1, 2, 3.5 & 5 days (respectively A, B, C & D) with different NaOH activation: 0s, 30s, 1 min & 5 min (a,b,c & d). D-e: Hydroxyapatite nanoparticles diffraction pattern.

A visible layer of minerals was deposited with an immersion time of 5 days. Residual deposited crystals were collected from the plastic cap (besides the PLGA samples. A sufficient quantity of these minerals (white powder) was extracted to make a XRD analysis of the mineral. **Figure 16** shows the diffraction pattern of the deposited crystals. Clear diffracted peaks appear and confirm the presence of Halite (NaCl salt) and hydroxyapatite.

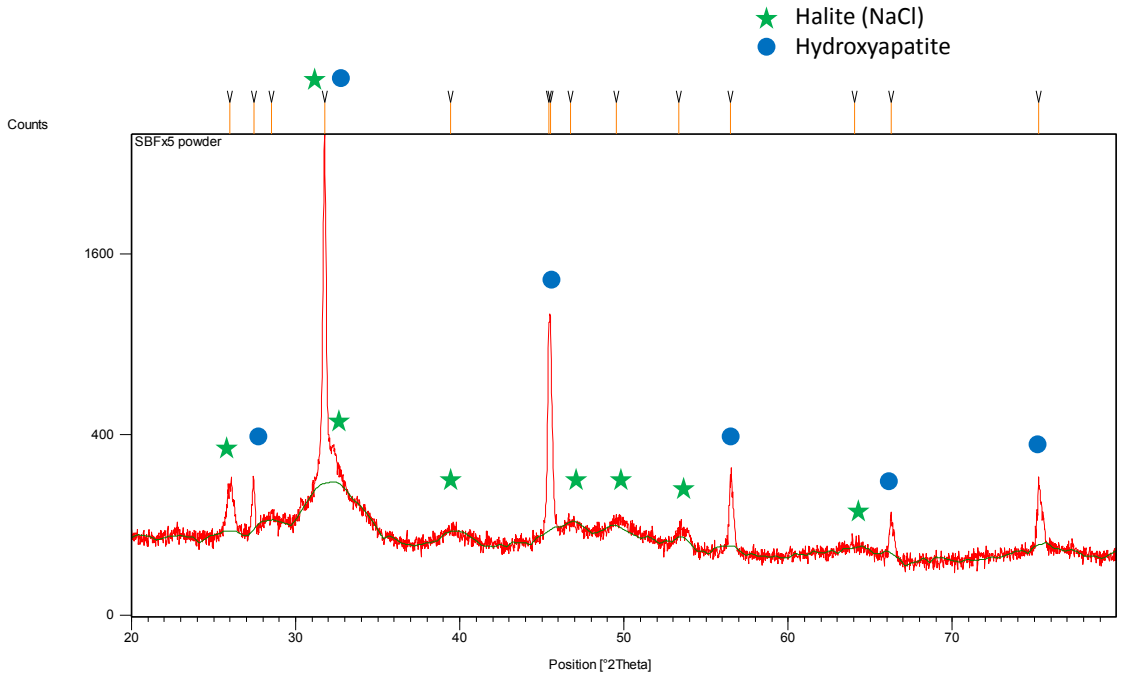

Figure 16 – XRD patterns of SBFx5 (5 days) deposited minerals (powder) showing Halite and hydroxyapatite diffracted peaks

All the SBF samples were characterized by XRD. Because they either do not present XRD peaks (SBFx1, 5 days) or because the matrices were too degraded for others characterization (SBFx1-21 days), only the most suitable samples were characterized by others techniques to obtain more details on morphology and composition of deposited minerals.

c) Jet Spray

Figure 17 shows the XRD graphics of jet sprayed matrices with an initial blend of PLGA and X% of hydroxyapatite nanoparticles. X value represents the percentage of HA nanoparticles incorporated inside the mixture. Comparing the patterns with that of HA particles (**figure 17-f**), diffracted peaks (2theta=26°, 31.8°, 32°, 33° & 34°) appear for samples containing more than 15% of nHA. We can observe an evolution of the peaks from 15% to 30%. Peaks are better defined with a higher intensity for those latter samples.

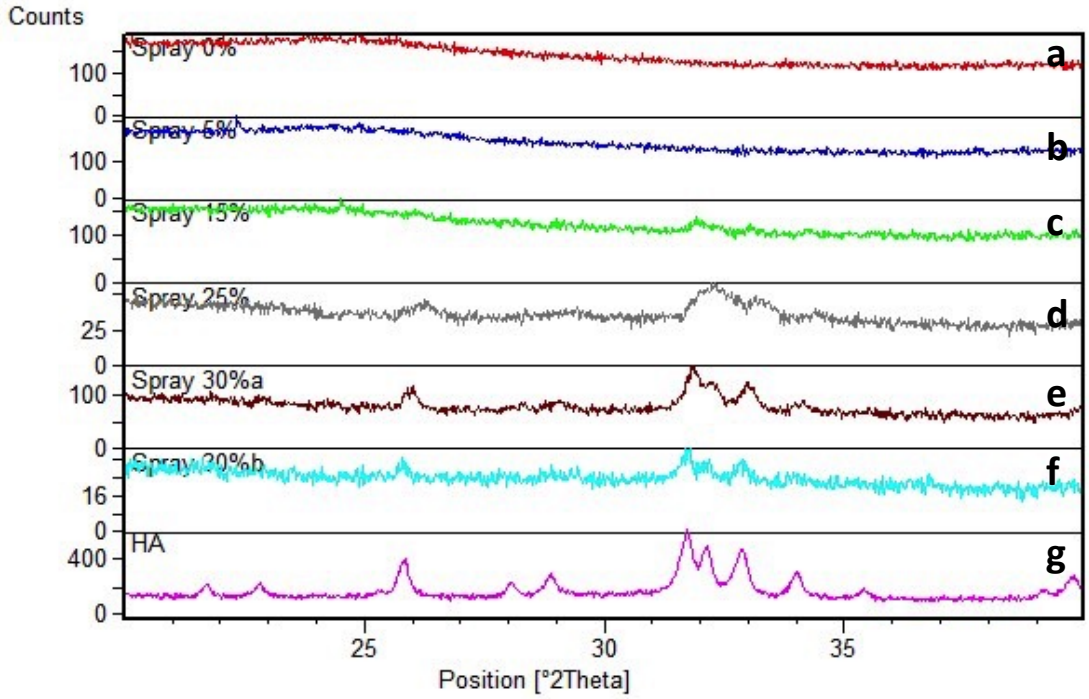

Figure 17- XRD patterns of JS PLGA matrices (PLGA+ X% nHA blend): 0%, 5%, 15%, 25%, 30%a & 30%b (a,b,c,d, e, & f)
f: Hydroxyapatite nanoparticles diffraction pattern
30%a and 30%b samples differ from the synthesis parameters (larger opening needle for 30%b (see table 6))

Observation:

During PLGA synthesis, some polymer mixture could accumulate at the end of the needle and form an aggregate. This kind of defects could be observed on some PLGA fibers produced by Jet spraying.

We could also observe that the synthesis time is depending on the proportion of nHA inside the initial blend. Time production increases with the nHA concentration, i.e. viscosity if the polymer. That could be easily explained by the higher force needed to form filament by Venturi effect.

PLGA matrices were removed from their grid at the end of the experiment and stored in a desiccator. Note that the PLGA fiber mat, depending on its thickness, is fragile and it could be sometimes difficult to take out from the grid an intact mat.

Nanoparticles inside the polymer solution tend to drop off at the bottom of the beaker when we stopped stirring. Even if the time of sedimentation is higher than the synthesis time of PLGA membrane, we may have a gradient of nHa concentration inside the initial polymer solution.

d) Co Jet spraying

Figure 18 shows the PLGA nanofibers produced by Co Jet spraying. None of the samples present clear diffracted peaks that could be related to a mineral phase.

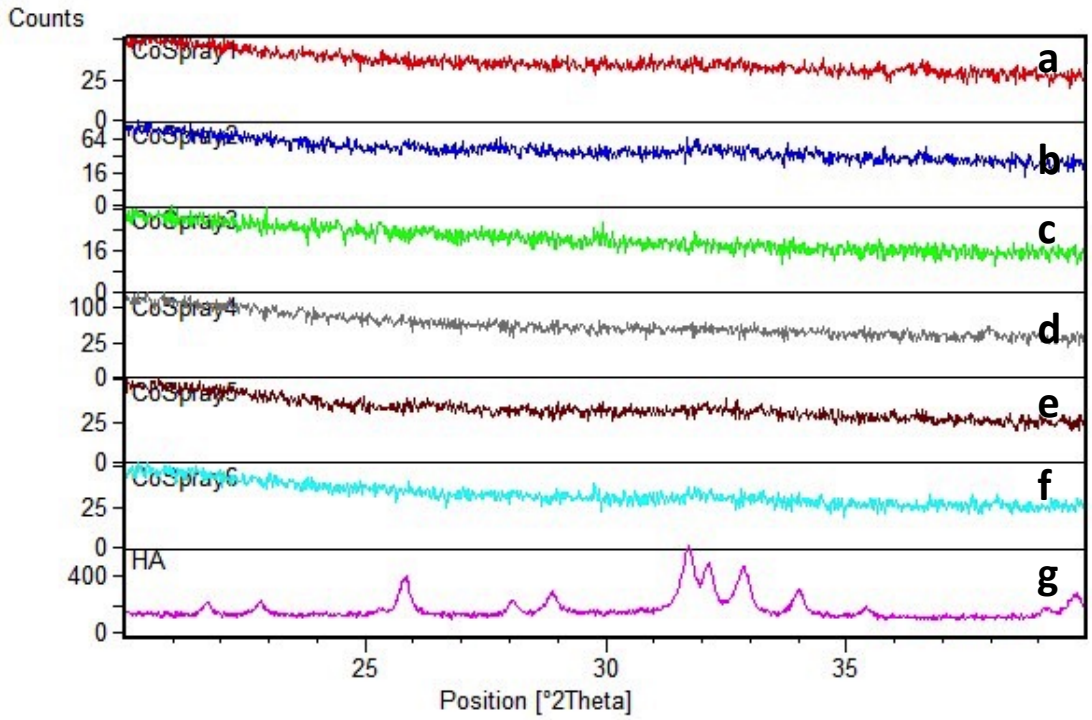

Figure 18 - XRD patterns of Co Jet Sprayed PLGA matrices (PLGA/Dichloromethane + nHA/water separated blends).
a: Sample n°1 (t1= 10min/t2= 10min)
b: Sample n°2 (t1= 27min/t2= 10min)
c: Sample n°3 (t1= 4min/t2= 11min)
d: Sample n°4 (t1= 5min/t2= 7min)
e: Sample n°5 (t1= 4min/t2= 12min)
f: Sample n°6 (t1= 4min/t2= 12min)
g: Hydroxyapatite nanoparticles diffraction pattern

Observation:

Nanoparticles in the water solution were aggregated at the bottom of the reservoir during the fiber synthesis. This problem of sedimentation is larger with water than the case of a mixture with PLGA solution.

2) Scanning Electron Microscopy (SEM) analysis

Electron microscopy is a powerful tool to observe morphologies and to identify different phases within small samples. We will determine in our case the microstructures of the deposited minerals previously detected by XRD technique.

a) Simulated Body Fluid x1

Three electrospun samples, treated in SBFx1 solutions, which XRD peaks were detected previously were characterized by SEM technique:

- SBFX1_1 day_0S (A)
- SBFx1_1 day_1min (B)
- SBFx1_7days_1min (C)

SEM images at a magnification of x300 (Figures 18-A, B, C and D) show the morphology of the electrospun fibers before and after SBF treatment. We could observe a relative alignment of the fibers on pictures B & C. However, on **figure 19-D,** PLGA nanofibres are more randomly positioned and seem entangled or laterally bonded. Besides that the fibers have higher average diameters.

Mineral structures could be observed on **figures 19-B', 19-C' & 19-D'** at a higher magnification (x1000). Crystals are present in small quantity and they are randomly distributed.

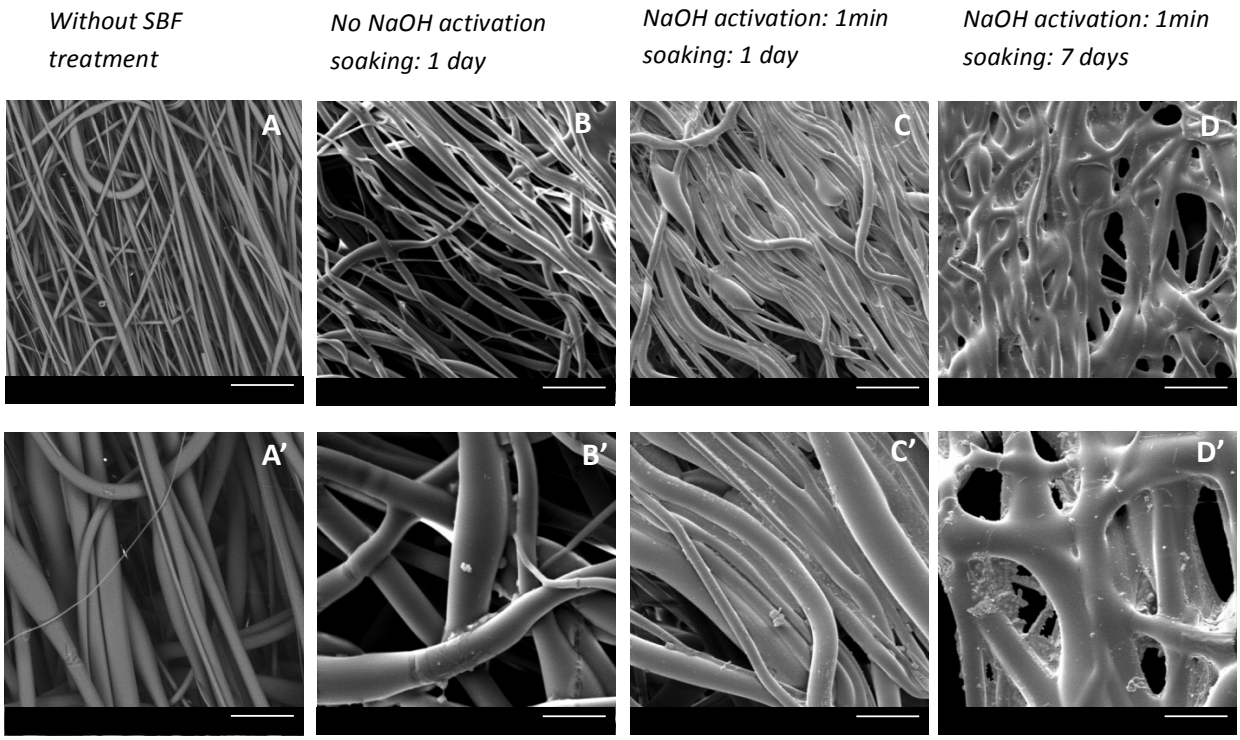

Figure 19 – SEM images showing the morphology of electrospun PLGA nanofibres after being exposed to different conditions:
A & A' – Electrospun PLGA nanofibres without SBF treatment (x300 & x1000)B & B'- SBF x1/0s of NaOH activation/SBF soaking during 1 day (x300 & x1000)
C & C'- SBFx1/ 1min of NaOH activation/ SBF soaking during 1 day (x300 & x1000)
D & D' - SBFx1/1min of NaOH activation/ SBF soaking during 7days (x300 & x1000).
Scale lines: 50 µm in A,B, C and D & 20µm in A´, B', C´ and D'.

Figure 20 shows EDX graphics corresponding to the mineral phases present at the fiber surface. Electron beam was focused on these crystals (arrows). Sodium (Na), Chorine (Cl), Carbon (C) and Oxygen (O) are the main components detected by EDX. C and O come from the PLGA polymer matrix that contains carbonated chains. The two others elements (Na and Cl) may come from an exterior deposition. The presence of Na and Cl in a quite important proportion suggests the precipitation of common Sodium chloride salt on the

polymer surface. We could notice in the EDX graphic B' the presence of Calcium (Ca) and phosphorus (P) peaks which are practically undetected in figure A' and C', possible consequence of a dissolution/recrystallization processes.

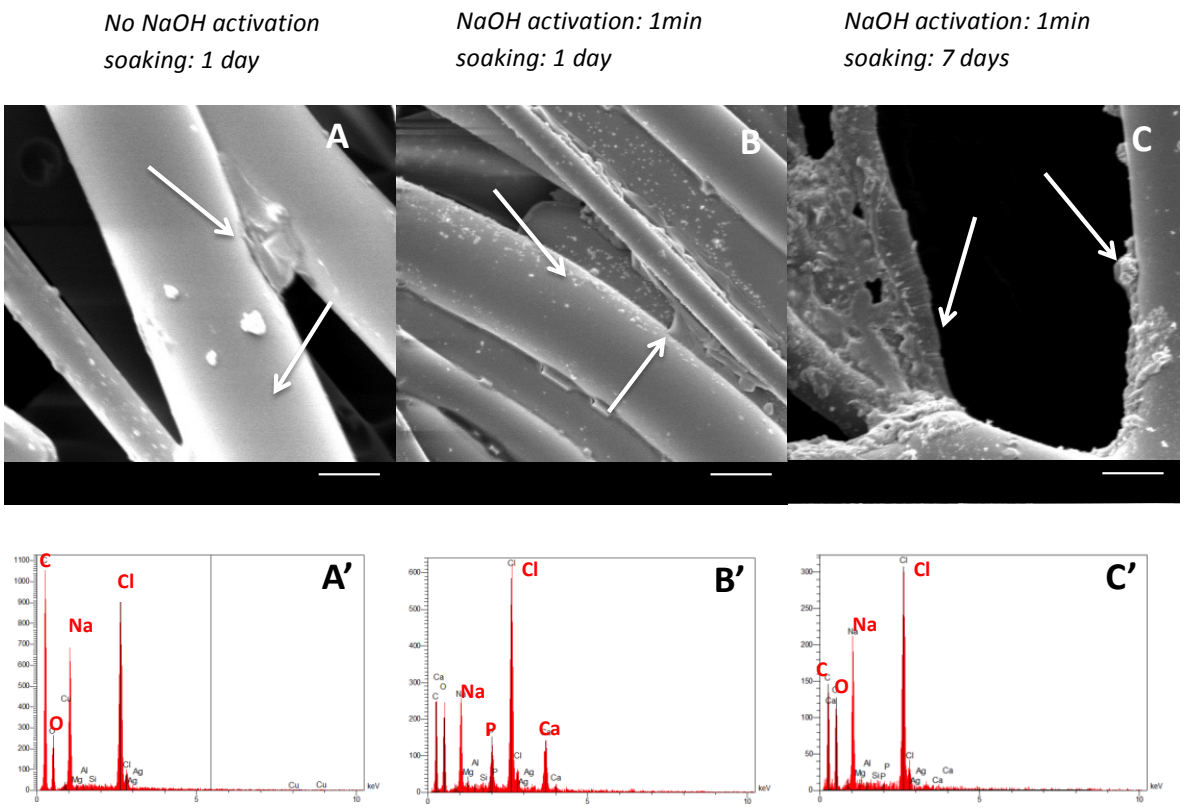

Figure 20 – SEM pictures of electrospun PLGA nanofibres after being exposed to different conditions and their respective EDX graphics probing the locally deposited crystals (arrows).

A: SBF x1/0s of NaOH activation/ SBF soaking during 1 day

B: SBFx1/ 1min of NaOH activation/ SBF soaking during 1 day

C: SBFx1/1min of NaOH activation/ SBF soaking during 7days

Magnification: x3000; scale line: 5 µm.

b) Simulated Body Fluid x5

Electrospun samples were characterized by SEM technique after undergoing SBFx5 soaking in the following conditions:

- A: SBF x5/5 min of NaOH activation/ *SBF soaking during* 1 day
- B: SBFx5/ 5min of NaOH activation/ *SBF soaking during* 2 days
- C:SBFx5/No NaOH activation/ *SBF soaking during* 3.5 days
- D: SBFx5/5min of NaOH activation/ *SBF soaking during* 3.5 days
- E: SBFx5/No NaOH activation/ *SBF soaking during* 5 days
- F: SBFx5/5min of NaOH activation/ *SBF soaking during* 5 days

Figure 21 shows the morphologies of electrospun PLGA nanofibres exposed to SBFx5 at a magnification of x300 and x1000.

A very small amount of minerals is deposited on the fibers surface for the samples soaked during 1 and 2 days in SBFx5 (A & B). Minerals could be only observed at a magnification of x1000. Bigger deposited minerals in white were found on the **figures 21-C and D** (3.5 days of immersion). Samples E and F soaked during 5 days present a uniform layer of minerals (**figure 21-E & F**).

SEM images at higher magnification (x3000) (**figures 22-A, B, C, D, E & F**) allow the analysis of the mineral phase.

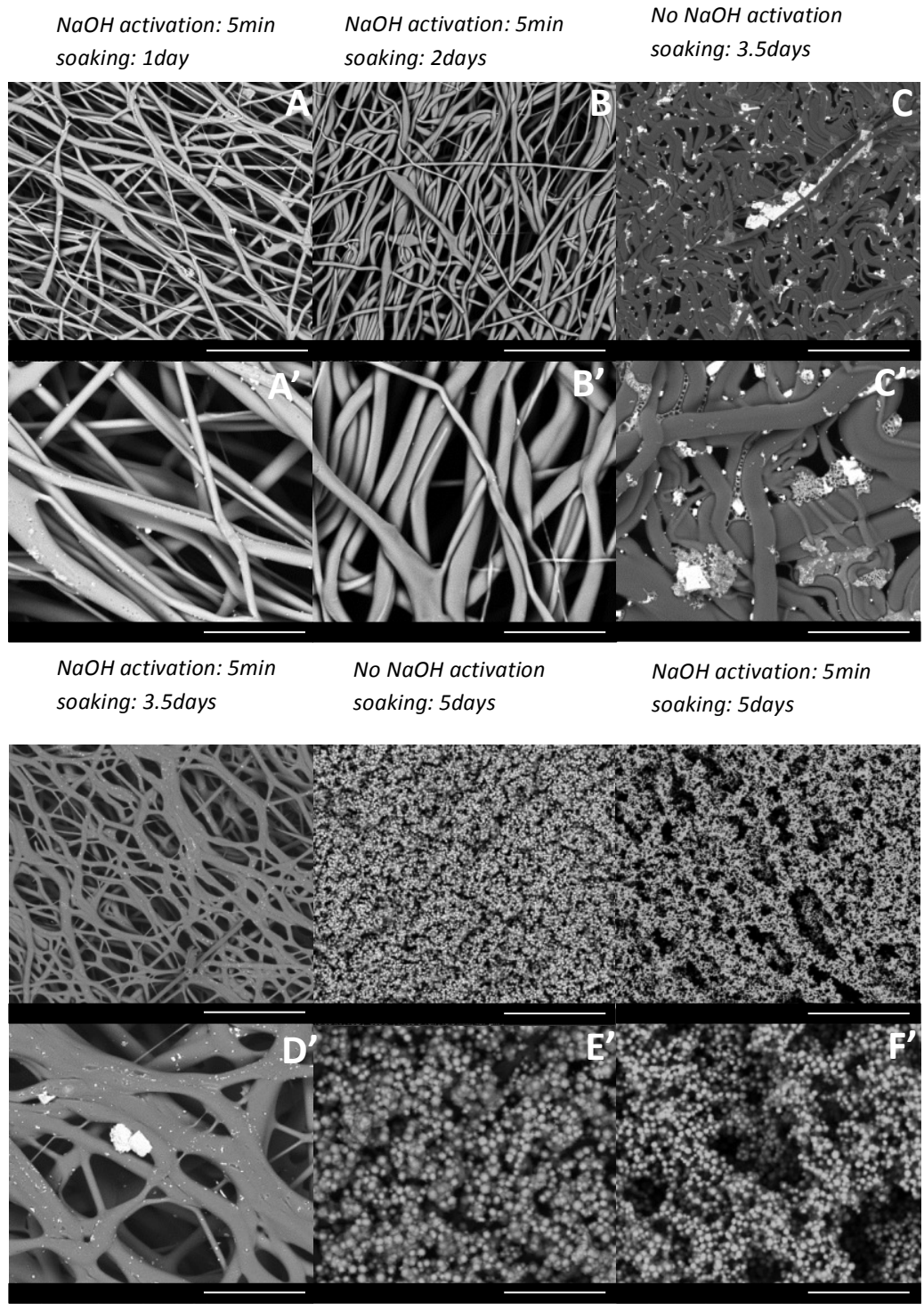

Figure 21 – SEM images showing the morphology of electrospun PLGA nanofibres after being exposed to different conditions:
A & A'- SBF x5/5 min of NaOH activation/1 day (x300 & x1000)
B & B'-SBFx5/ 5min of NaOH activation/2 days (x300 & x1000)
C & C' - SBFx5/No NaOH activation/3.5 days (x300 & x1000)
D & D'- SBFx5/5min of NaOH activation/3.5 days (x300 & x1000)
E & E'- SBFx5/No NaOH activation/5 days (x300 & x1000)

F & F'- SBFx5/5min of NaOH activation/5 days (x300 & x1000)
Scale lines: 100µm for x300 & 50 µm for x1000
Scale lines: 50µm (A, B, C, D, E, F & G); 100µm (A', B', C', D', E', F' & G')

For the samples with an immersion time smaller than 5 days, EDX spectra proved the presence of several elements such as Sodium Na, Calcium Ca, Chlorine Cl and even Magnesium Mg. We can say that there are some minerals depositions including NaCl (**figure 22-C'**) and maybe some Calcium minerals did take place (**figure 22-D'**).

However, crystals formed on PLGA matrices immersed during 5 days inside SBFx5 solution clearly contains Calcium and Phosphorus elements (EDX graphs on **figures 22- E' and - F'**) in addition to Carbon and Hydrogen (detected because of PLGA presence). This analysis confirms the formation of calcium phosphate crystals on the PLGA fibers for the samples E and F.

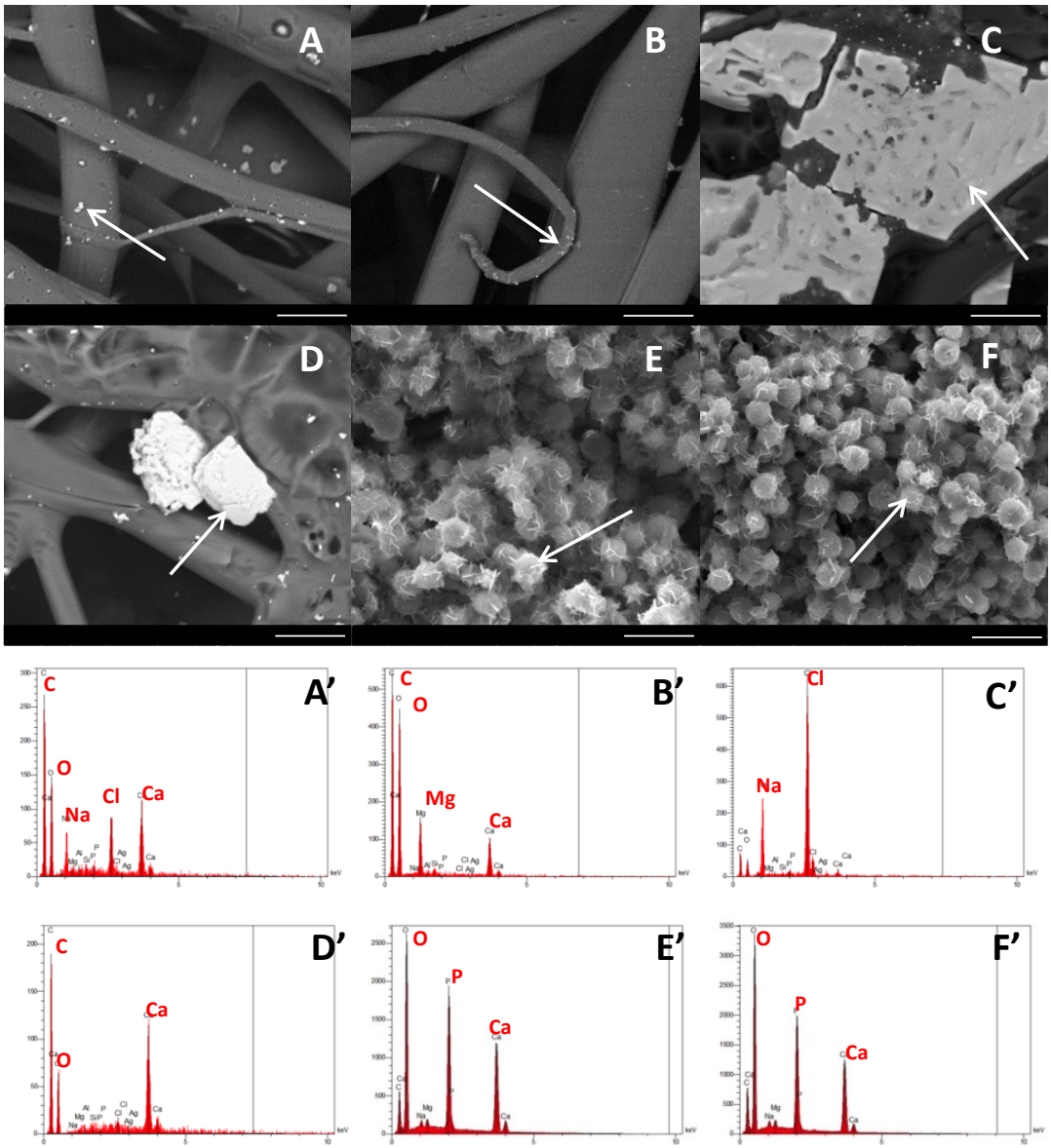

Figure 22– SEM pictures of electrospun PLGA nanofibres after being exposed to different conditions and their respective EDX graphics probing the deposited crystals (arrows). Scale line (10µm)

A: SBF x5/5min of NaOH activation/1 day

B: SBFx5/ 5min of NaOH activation/2 days

C : SBFx5/No NaOH activation/3.5 days

D: SBFx5/5min of NaOH activation/3.5 days

E: SBFx5/No NaOH activation/5 days

F: SBFx5/5min of NaOH activation/5 days

SEM images with a higher magnification (x25 000) were obtained on the samples SBFx5 with 5 days of immersion. **Figure 23** shows the characteristic structures of the deposited minerals. Small spheres were formed with diameters between 2 and 5 µm and they present sharp extremities on their surfaces.

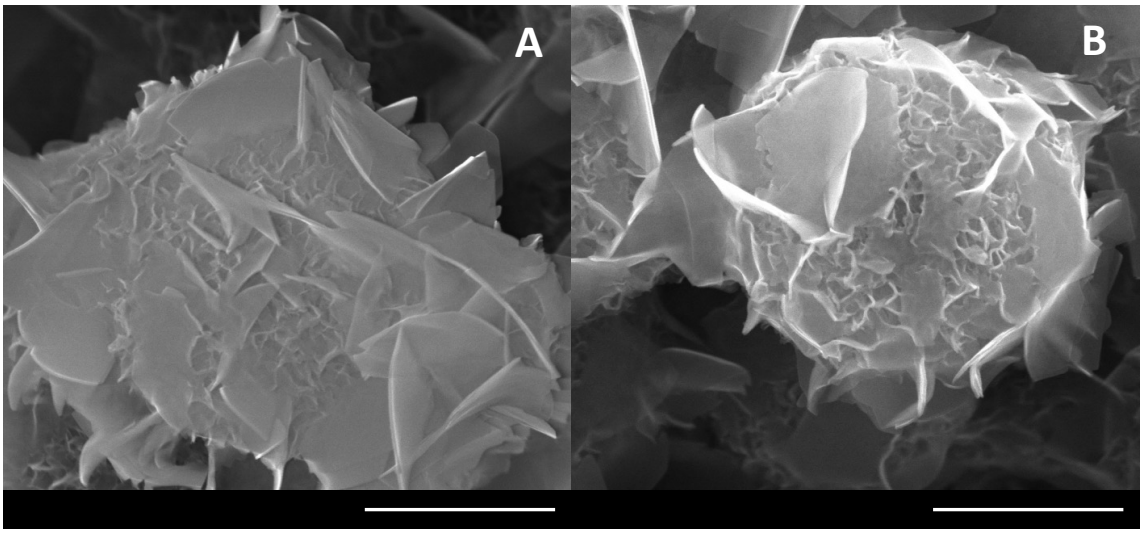

Figure 23– SEM images (x25 000) of SBFx5_5 days immersion without (A) and with NaOH activation (5min) (B) – Scale line (2 µm)

c) Jet spraying (PLGA+nHA initial blend)

Figure 24 reveals the SEM images of the PLGA matrices produced by the Jet spraying technique (initial mixture of nHA + PLGA). The magnification of x300 allows us to

visualize the fibers morphology. All samples present a complex and disordered polymer fibers network with some defects (beads). The density and the disorder of the fibers seem to be larger when we increase the percentage of nanoparticles (**figures 23-D, E & F**). The average diameters of the fibers are between 0.5 and 2 µm.

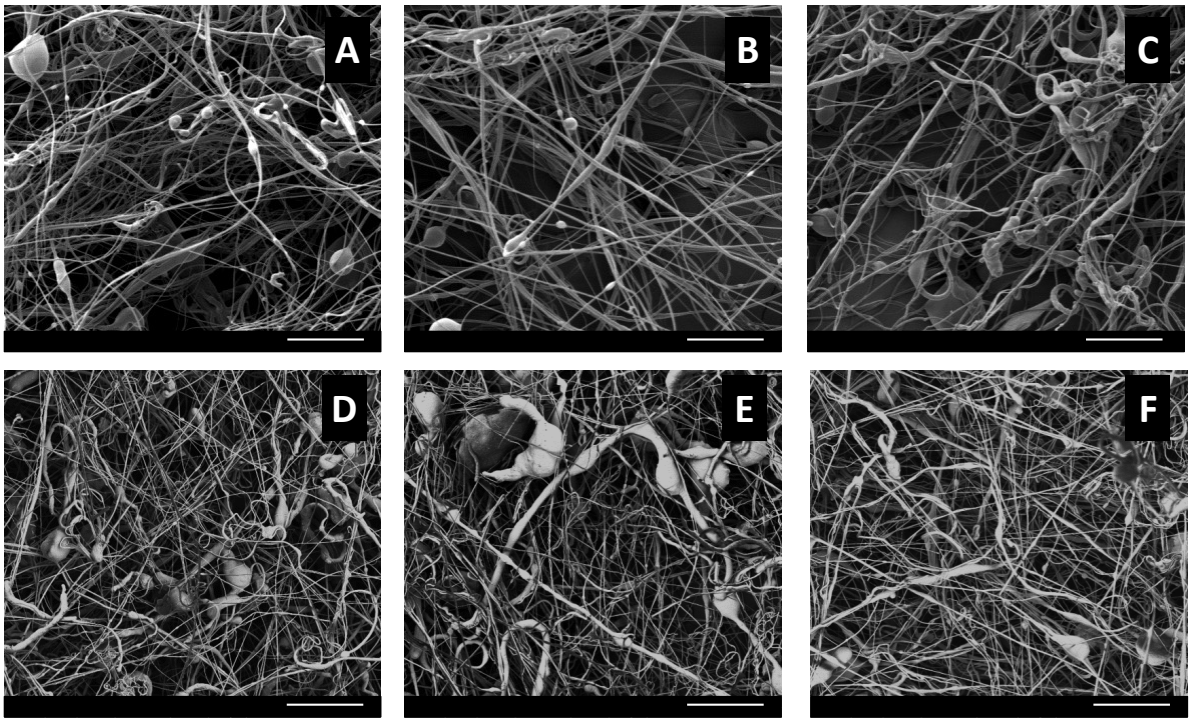

Figure 24– SEM images (x300) showing the morphology of PLGA+X%nHA nanofibers produced by Jet spraying. The concentration values (X%) of nHA are : 0%(A), 5%(B), 15%(C), 25%(D), 30%a(E) and 30%b(F).
30%a and 30%b samples differ from the synthesis parameters (larger opening needle for 30%b (see table 6)).
Scale lines: 100 µm

Figure 25 shows the SEM pictures and EDX micrographs of the jet sprayed samples with the highest amount of hydroxyapatite nanoparticles (25%, 30% with different synthesis parameters) (**A, B & C**). EDX measurements were performed on the mineral

salts (the probed sites are pointed out by arrows on the SEM images). They present peaks for calcium and phosphorus elements, confirming the presence of calcium phosphate.

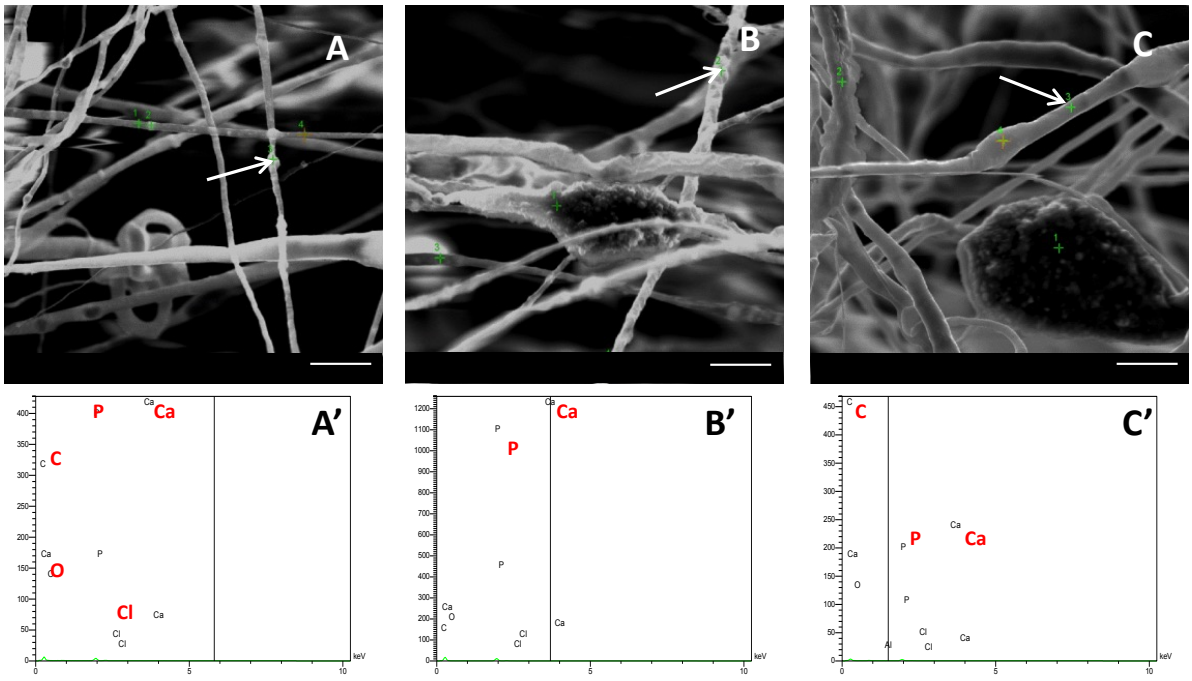

Figure 25 – SEM images (BSE mode/x3000) of jet-sprayed nanofibres and their respective EDX graphics pointed on the deposited crystals (arrows). Scale line: 10 µm A=25%/B=30%a & C=30%b

d) Co Jet spraying

SEM images (x300, x1000 & x3000) of co-Jet sprayed nanofibers show the deposition of the nanoparticles at the PLGA surface (**figure 26 & 27**). Hydroxyapatite nanoparticles (nHAs) appear in white on the SEM images. **Figure 28** shows at a higher magnification the deposited nanoparticles of hydroxyapatite on the PLGA jet sprayed fibers. The average diameters of the fibers are still ranging from 0.5 to 2 µm as with the previous jet spraying experiment.

Depending on the Jet spraying parameters, sprayed nanoparticles are differentially distributed on the surface of the PLGA surface. nHAs tends to form small agglomerates

and cover only some parts of the fibers. We can observe that with a higher nozzle opening (> 1.39) (sample 3, 4 & 5/ **figure 27**) there is a larger concentration of nanoparticles (in white) at the surface of the polymer fibres. Comparing the images on **figure 27**, it seems that we have denser matrices for the sample 5 and 6 (**figure 27-B & C**). The increase of density might be due to the change of the synthesis parameters: the pressure was deceased to 6 Bar for samples n°5 and 6.

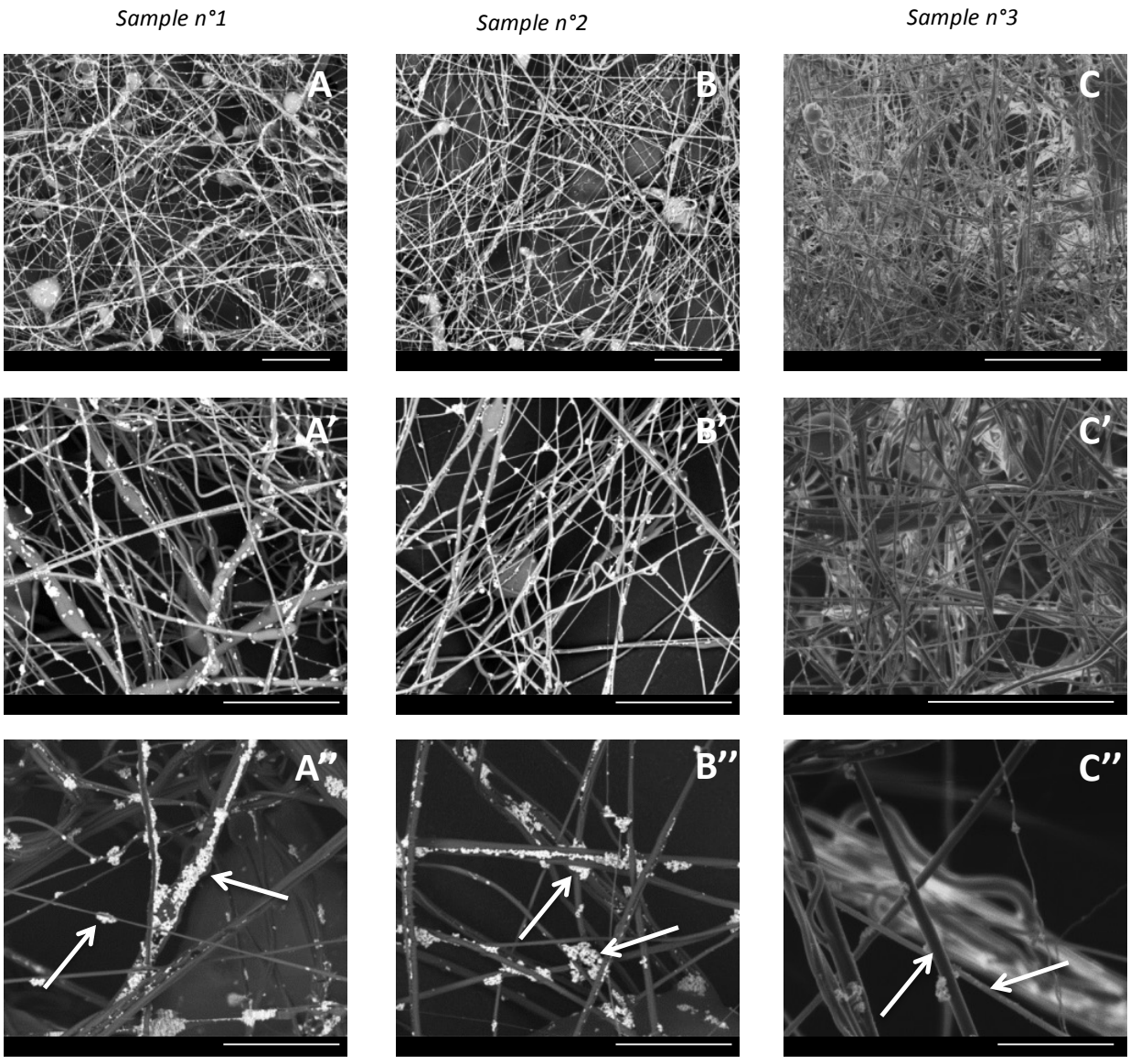

Figure 26 – SEM images (x300, x1000 & x3000) of Co Jet Sprayed matrices with different synthesis parameters:
Sample n°1 (A): Nozzle opening: 1.3 mm/nHA concentration: 1.85mg/mL/ pressure gun 2:

10 bars

Sample n°2 (B): Nozzle opening: 1.3 mm/nHA concentration: 1mg/mL/ pressure gun 2: 10 bars

Sample n°3 (C): Nozzle opening: 1.29 mm/nHA concentration: 1mg/mL/ pressure gun 2: 10 bars

Scale bares: 50µm (A,B & C) 20µm (A',B' & C') 5µm (A'',B'' & C'')

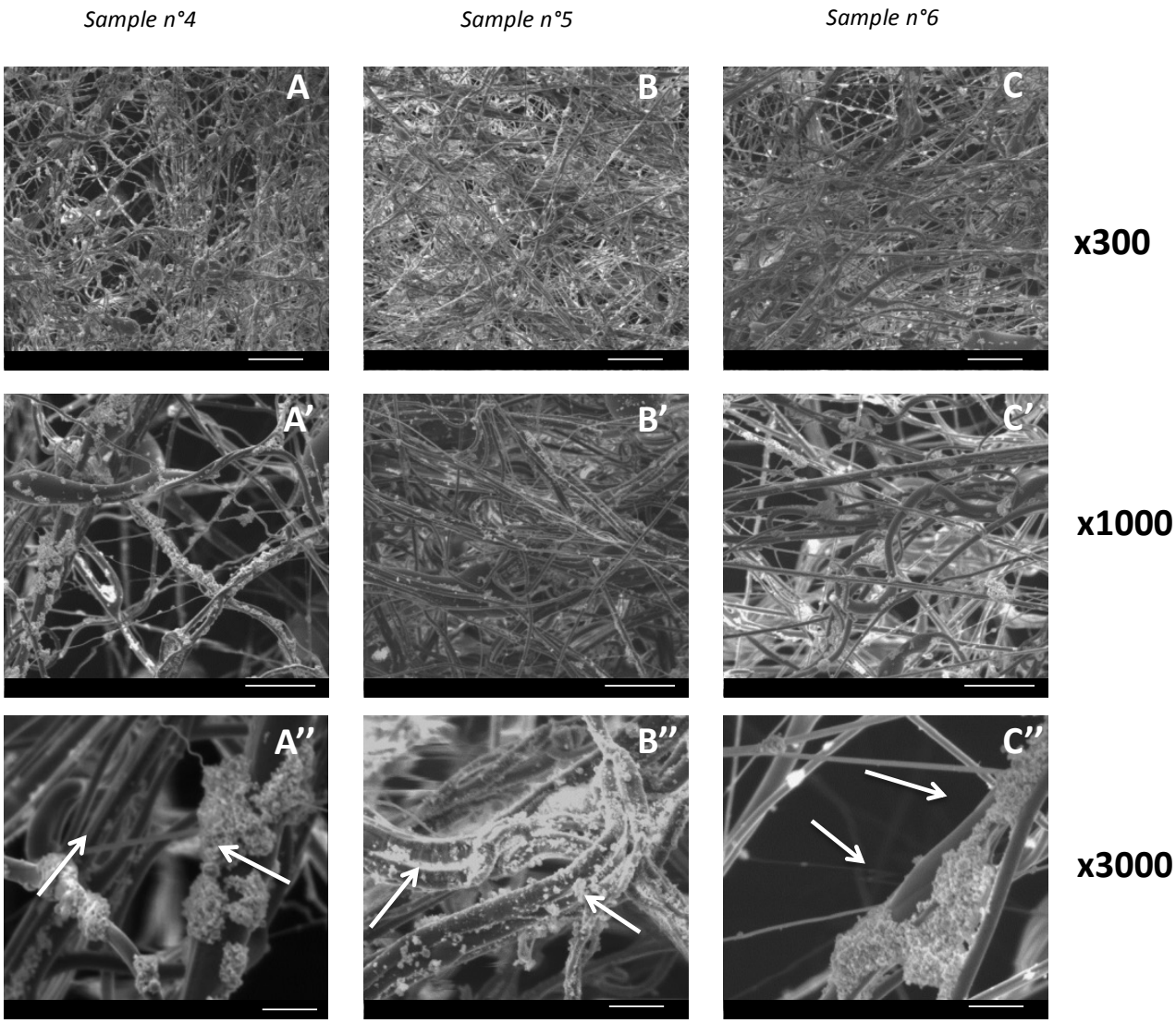

Figure 27 – SEM images (x300, x1000 & x3000) of Co Jet Sprayed matrices with different synthesis parameters:

Sample n°4 (A): Nozzle opening: 1.39 mm/nHA concentration: 1mg/mL/ pressure gun 2: 10 bars
Sample n°5 (B): Nozzle opening: 1.35 mm/nHA concentration: 1mg/mL/ pressure gun 2: 6.5 bars
Sample n°6 (C): Nozzle opening: 1.45 mm/nHA concentration: 1mg/mL/ pressure gun 2: 6.5 bars
Scale bares: 50µm (A,B & C) 20µm (A',B' & C') 5µm (A'',B'' & C'')

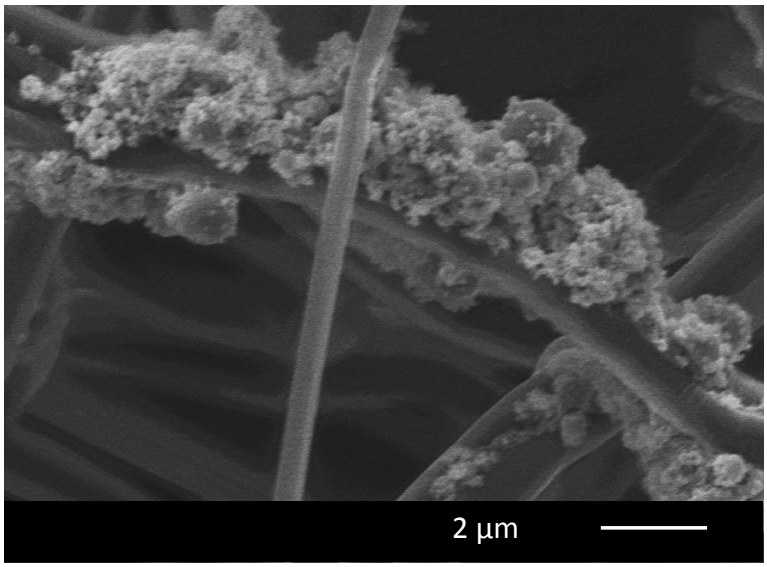

Figure 28 – SEM image of hydroxyapatite nanoparticles at the surface of jet sprayed PLGA fibers. Sample n° 3. Scale bare : 2 µm

3) Degradation test

Table 9 summarizes the obtained values. Samples are jet-sprayed matrices (**method 2**), with different contents of HA nanoparticles.

Table 9 – Size evolution of the jet-sprayed PLGA samples after immersion in PBS solution during 21 days.

Samples	X change %	Y change %	Average %
1. PLGA + 5% HA	-87.5	-94.8	-91.1
2. PLGA + 15% HA	-81.5	-95.2	-88.4
3. PLGA + 25% HA	-79.4	-86.1	-82.8
4. PLGA + 30% HA	-50.6	-65.2	-57.9
5. PLGA + 30% HA	-56.2	-74.2	-65.2

An important shrinkage of the PLGA matrices can be observed. PLGA matrices containing a percentage of HA inferior to 25% have a reduction superior to 80%. The structure quality of the composite is damaged. However, with higher percentage of HA nanoparticles, the shrinkage phenomenon is reduced to 60/65%.

IX - Discussion

Simulated Body Fluid experiments

SBF experiments were usually considered useful in predicting the biomaterials bioactivity *in vitro*. It is believed that the crystal growth of hydroxyapatite induced by SBF occurs in two main steps: nucleation and particle growth (52). The thermodynamical instability of the SBF solutions may promote an easy crystal deposition.

There was no deposition of minerals with the first SBFx1 solution regardless the immersion time period. Only a few crystals were observed on the SEM images (**figure 20 p.57**) that indicate a low bio-mineralization by SBFx1. Furthermore, minerals were not formed in a sufficient proportion to be detected with the X-Ray diffraction technique. Graphs do not present clear diffracted peaks allowing the recognition of a crystalline structure. On three SBFx1 samples, a small diffracted peak can be observed around 2theta = 31.8/32 °.This peak can be related to both hydroxyapatite (2theta=31.774) and Halite (NaCl) (2theta=31.820) crystal structures. The broad width of the peak (due to the low precision of the measure (i.e. non complete flatness of the sample)) does not allow the differentiation of the two crystals. However, later EDX measurements determined the presence of Na and Cl elements, demonstrating the formation of NaCl only on the fibers. Some researchers obtained the deposition of calcium phosphate minerals with SBFx1 solution (26). Francisco Valenzuela et al. also demonstrated the presence of NaCL minerals by EDX measurements (28).

We observed during the immersion period small leaks around the plastic cap of the SBF containers. An incomplete isolation of the recipient caused a precipitation between the cap and the plastic container. A phenomenon of nucleation triggered a localized precipitation. The nucleation of the minerals can be selectively induced by thermodynamic properties (scratch on the edges of the containers (19) or contact with the extern environment). According to the theory (52), as soon as a critical radius is reached, calcium and phosphate ions are attracted toward the first nucleates and not to

the fibres surface. Kinetic/thermodynamic competition process can be an explanation of the non-homogeneous formation of the salts. Plastic containers are made of polypropylene.

Structures of the electrospun PLGA matrices are damaged during their immersion in SBF solutions (x1 and x5). The degradation of the fibers is directly related to the time of immersion. Hydrolysis of the PLGA polymer (**figure 29**) damages the fibres and degrades physical properties. After 7 days of immersion, it was more difficult to remove the PLGA samples from the plastic cap of the SBF container (films stuck on the cap). The degradation behaviour was noticeable by the difficult manipulation of the samples, which increased over incubation time. For an immersion of 21 days, it was not possible to remove the samples without damaging the fibers. Only sample fragments were collected, allowing a XRD powder characterization. As a result, SBF immersion times have to be shorter than 7 days in order to not lose the physical integrity of the nanofibrous scaffolds. The difference of degradation between the SBF X1 and X5 were not observed on shorter times.

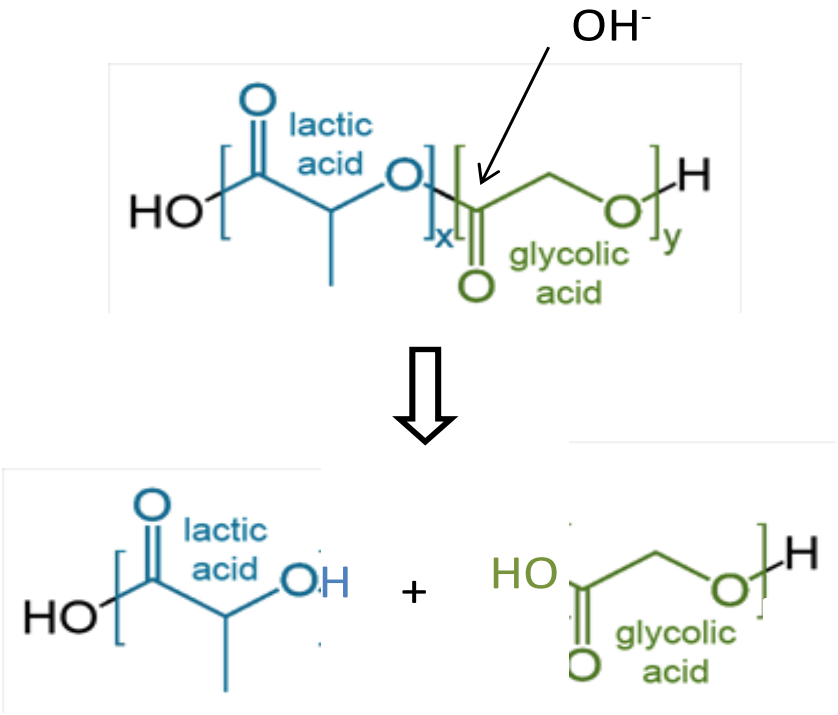

Figure 29 – PLGA hydrolysis mechanism

SEM images of 7 days immersion samples show the degradation effects on PLGA nanofibers. **Figure 18 (p.54)** shows the loss of the fibers alignment, the smoother surface of the PLGA fibers due to the PLGA hydrolysis. Joanna Buczynska et al.'s (32) analysed the mechanical properties evolution of PLLA fibers depending of the immersion time in a SBFx3 solution. PLGA fibers were weakening with an increasing immersion time. Average diameters increased (due to the minerals coating) but strain to failure or tensile strength decreased.

Degradation tests performed in PBS solution with jet-sprayed fibers showed a considerable shrinkage (> 80%) of the PLGA matrices after 21 days of immersion. These data confirmed that, even with HA presence inside the nanofibers, PLGA membrane are considerably affected by hydrolysis over long period of immersion (7 > days). Young You at al. (53) observed in their works the degradation of electrospun PLGA nanofibers in PBS. Degradation of PLGA matrices were shown by Scanning Electron Microscopy over 8 days of immersion whereas no significant morphological changes were noticed for the first 4 days of degradation.

The metastable solutions SBFx1 and SBFx5 were difficult to synthesize. The high proportion of ions in solution makes the SBF solutions hard to prepare and to conserve. Many researchers prepared super saturated solutions in order to increase the nucleation rate of mineralization (38). To maintain the metastable condition of SBF solution and to keep it as limpid solution at 37°C, a low pH is necessary, around 6.4 for SBFx5.

Even with the pH difference between SBFx5 and natural blood plasma (pH~7.2/7.4), some researchers performed mineralization tests at such low pH (37), (33). Several techniques are used to make a solution with high ionic concentrations. Some synthesize their SBF solutions with a CO_2 reflux system in order to lower the pH below 7 through a new input of HCO_3^-/$H2CO_2^-$ and thus increase the solubility of the compounds (54).

In our study case, we increased the SBF salts solubility by lowering the pH at 6.4. With mineralization through normal SBF, we cannot obtain mineralized PLGA matrices with good remaining physical properties. Mineralization seems to be too slow to preserve

the integrity of the nanofibers. However, SBFx5 solutions allow us to shorten the immersion time and obtain a faster mineralization without compromising the properties of the substrates. Indeed, even if the hydrolysis process is accelerated by the lower pH of the solution SBFx5 (pH=6.4) (acidic media should accelerate the hydrolysis of degradable polymers), mineralization is faster. Thus this may have a positive contribute towards PLGA properties maintenance and “protect” the fiber from hydrolysis.

Significant mineral deposition was observed on SBFx5 PLGA samples after 3.5 days of immersion. EDX graphs show the formation of Halite and Calcium Phosphate minerals by detecting the main elements (Na, Cl, Ca, P and O). Two different structures may be differentiated on the samples SBFx5_3.5 days of immersion. A rectangular crystal structure as shown on **figure 21-C (p.59)** might correspond to NaCl minerals (55), (56) whereas a more shapeless crystal (**figure 21-D**) contains Ca elements.

A uniform layer of minerals seems to be deposited on the SBFx5_5 days immersion samples. A large part of the PLGA fibers is recovered by calcium phosphate crystals (presence of Ca and P elements on EDX graphs). Similar homogeneous deposition results were obtained with SBF mineralization: layers of calcium deficient phosphate on PLLA nanofibers with SBFx5 (33), small CaP layer around PLGA fibers with SBFx10 (38). SEM images on **figures 20-E & F (p.57)** do not allow with certitude the presence of pores. The deposited minerals reduce and maybe eliminate the initial porosity of the fibers. The deposited powder was examined through X-Ray diffraction (**figure 16 p.51**). Two main crystallise phases appeared very distinctly, Halite (NaCl) and hydroxyapatite. The ratio of Ca/P was measured for the sample SBFx5 5days of immersion. Average Ca/P ratio around 1.4 was determined with the EDX data. In comparison with the apatite material (Ca/P=1.67), the mineral presents at the surface of the PLGA membranes is calcium deficient. The deposited minerals do not correspond to a pure hydroxyapatite layer.

It was often observed that amorphous calcium or calcium deficient minerals are first formed during SBF mineralization (SBFx5/ soaking times: 6h, 18h & 24h; (34)). CaP phases precipitated in aqueous solutions mainly include dicalcium Phosphate [$CaHPO_4.2H_2O$] (DCPD), octocalcium phosphate [$Ca_8(HPO_4)_2(PO_4)_4$ $5H_2O$] (OCP),

hydroxyapatite [$Ca_{10}(OH)2(PO_4)_6$] (HA). (52) HA is the most thermodynamically stable mineral in physiological environment. OCP and DCPD are believed to be precursors of HA. Because they grow faster than HA (kinetically favourable), they will first precipitate on the surface on the PLGA layers and then transform into HA. According to thermodynamic and kinetics crystal growth simulation (52), HA has a negative free energy, which means a favourable precipitation, when pH > 5.4. However, OCP and DCPD have faster nucleation rates than HA. It should be noted that the difference in nucleation rate between HA and OCP increases when the pH decreases. In our case where the pH is around 6.4, it should be normal to observe first a deposition of calcium deficient minerals.

Calcium phosphate on SBFx5 5days samples was formed under a characteristic shape. **Figure 23 (p.62)** shows the structure of the deposited mineral as hemispherical-shaped apatite granules (diameters around 5 µm) with a rough surface containing needle like crystals. Such flaky structures were previously observed in SBF mineralization (24), (33), (57). Needle shaped structures are usually composed by a mixture of hydroxyapatite and calcium deficient phosphate dehydrated. CDCP being considered as precursors of the apatite formation, they lower the Ca/P ratio (34).

NaOH activation was performed on the PLGA samples in order to create specific sites promoting the apatite formation. Tristan I. Croll et al. (27), estimated NaOH activation by measuring the contact angle on PLGA surfaces. The roughness of the surface varied only at the very beginning of the activation (orders of seconds). To selectively activate the surface of the polymer, we therefore choose short times of treatment (0s, 30s, 1min and 5min), with the aim of not degrading the polymer in the matrices depth. It was demonstrated that NaOH activation has a very fast effect on PLGA. Others activation processes could have been performed on polymers to promote mineralization. For instance, F. Yang et al. (58) and Xiaoran Li et al. (57) used an argon plasma treatment during 10 minutes to activate the surface of their polymers (PCL and PLGA).

There were no relations between the NaOH pre activation and the observed mineral deposition, for both SBF solutions. SBFx1 solution was not enough concentrated in order to prove the effect of NaOH activation.

For SBFx5 mineralization, a sufficient minerals deposition was not observed for short immersion times (< 5 days). However, a semi quantitative analysis can be done with the evolution of the XRD spectra for 5 days of immersion. On **figure 15-D (p.50)**, there is a small increase of the diffracted peak (2theta= 26°) with NaOH activation. Indeed, on the graph **c** and **d**, the characteristic peak could be differentiated from the noisy background. This could be explained by the activation of the NaOH liquid on the PLGA fibers. More precise characterizations have to be performed to confirm the real effect of NaOH activation. We cannot see a real difference between the mineralization of SBFx5 samples (0s and 5 minutes NaOH activation) on the SEM images (**figures 21-E & F p.59**). It is hard to achieve a quantitative analysis because the minerals were deposited homogenously and cover all the fibers. Comparing **figures 20-C & D** (p.57) (at the same magnification), it comes out that NaOH activation seems to facilitate the "diameter decrease" of the fibers. As the PLGA hydrolysis should be induced by NaOH, it is plausible that we have a higher degradation, i.e. fast decrease of the fiber diameters.

Jet-spraying technique

Jet-Spraying techniques allow the construction of a functional three dimensional matrix. PLGA nanofibers networks were designed with an adequate porosity for tissue regeneration (around 90%). Jet-Spraying is also a good method to compute and incorporate ceramic fillers, in our case, apatite, to the fibers. Nanoparticles can be easily introduced in a controllable way into the PLGA polymer. In theory, ceramics fillers can be inserted at a specific place inside the PLGA network, either to produce several composite layers or to mineralize only on the surface of the sample. In the present work different contents (up to 40%) of nHAs were incorporated by the jet-spraying technique (blend mixture) and the presence of calcium phosphate was checked by x-rays diffraction and SEM analysis. SEM images (**figure 23 p.62**) show the insertion of nanoparticles inside the

polymer fibers. The initial mixture (nHA + polymer) projected on the grid offers the good incorporation of the fillers. Similar results, where HA nanoparticles are included inside the PLGA fibers, can be obtained with the electrospinning technique (F. Yang with 0, 25 & 50%wt of nHA/fiber diameter: 0.32 to 0.43 µm (21)).

Depending of the preparation parameters and the proportion of fillers, we were able to create a nanocomposite with fashionable properties. Depending on the amount of HA incorporated into the fibers, the physicals properties will be slightly changed. Yang et al. (21) realized mechanical tests on their PCL/nHA composites. It was shown that the addition of nHA increased the tensile stress, ductility and toughness. This mechanical reinforcement effect can be due to an additional energy-dissipating mechanism introduced by the nanoparticles. Valenzuela et al. (28) carried out mechanical tests on alginate/ nHA nanocomposite and showed that a maximum nHA content of 25% inside the polymer offers the best physical properties. HA nanoparticles make the nanofiber matrix more stiff and less plastic in deformation, which is the typical characteristic of hard inorganic fillers. Consequently, stiffness of the supporting scaffold can be easily adjusted by varying the proportion of nHA.

nHA incorporation has an effect on bioactivity and cell proliferation [28]. ECM organization and production are highly influenced by the presence of apatite nanoparticles. In Li‘s paper (27), *in vitro* experiments on an electrospun nHA/PLGA composite were performed. Human osteoblast cells were cultured during 14 days on the scaffold and confocal fluorescent microscopic images allowed the observation on an enhancement of cell proliferation (in comparison with a simple PLGA matrix). HA nanoparticles have a non-negligible effect on cell biocompatibility and Yang (21) also proved that hydroxyapatite provides a suitable environment for osteoblast-like cell differentiation and proliferation.

Mineralization assays, like formation of apatite with prolonged SBF immersion (up to 4 weeks), were performed on HA/polymer composites in order to characterize the amelioration of the bioactivity. Yang demonstrated that the presence of HA nanoparticles

have a great influence on apatite formation. This effect can be attributed to the partial dissolution of nHa and thus the release of calcium ions which favors apatite formation or the exposure of nHA particles on the polymer surface providing nucleation sites for apatite growth. Sang et al. also observed that HA nanoparticles act as catalyst to mineral deposition on porous polymer/ceramic composite scaffolds (29).

In our case, the non-homogenous repartition and aggregates formation has to be solved by adjusting the spraying parameters. Further tests should be realized in order to optimize the quality of the fibers. However, these first experiments prove the feasibility of the nano composite synthesis techniques by jet spraying and their promising outcomes.

Co Jet Spraying

The third mineralization technique allowed the partial coating of HA nanoparticles on the PLGA fiber surfaces. The separated projection of polymer solution and nanoparticles was not reported in the literature. The novelty of this method is that a layer of HA nanoparticles can be deposited at the surface of nanofibers. The co projection of the nanoparticles and the polymer may be a great alternative to cover the polymer scaffold and enhance the bioactivity of the all system. Contrary to the previous composite, hydroxyapatite will be directly in contact with the ECM. The effect might be more efficient for implant integration. The experiments showed the feasibility of the synthesis method. Even if the parameters have to be further adjusted, we were able to design a promising nanocomposite. Nanoparticles were not distributed homogenously on the fibre surfaces and some aggregates were formed, decreasing the quality of the nanofibres. The non-complete covering can be due to the characteristic structure of the nanoparticles. Their hexagonal prisms shapes might influence the deposition process because of steric constrains. Thus, it may be interesting to project HA nanoparticles with different shapes and sizes (nHap may be produced as very thin particles with a needle or plate like shape). Further tests should be done in order to check the mechanical and

biological properties of the new composite. Especially the adherence of the nanoparticles to the surface via soaking tests should be tested to provide a viable biological system.

Others characterization techniques non-available in the laboratory, could be done to improve the analysis of the mineralized PLGA nanofibers. For instance, Fourier Transform InfraRed spectroscopy may provide new data about the deposited minerals on the SBF samples. Indeed, with the XRD techniques, we did not collect diffraction for amorphous phases. Consequently, we are not able to assure the non-presence of amorphous calcium phosphate, known as a precursor of HA in mineralization process. BET (Brunauer–Emmett–Teller) measurements will also provide interesting data about the specific surface area and the porosity of our materials. Finally, thermogravimetric analysis (TGA) would allow the determination of the exact amount of minerals we managed to precipitate (SBF) or incorporate (jet spray) inside the different PLGA nanofibers.

X - Conclusion/Perspectives

Mineralized PLGA nanofibres were successfully produced through 3 different methods. SBF mineralization and co jet-spraying techniques allowed the formation of a calcium phosphate deposit around PLGA nanofibers whereas jet spraying created a nanocomposite where nanoparticles were included inside the core of the fibers.

These two types of configuration offer different potential advantages for guided tissue engineering applications. Mineralization at the surface of the fibers will provide bioactivity to the scaffold by promoting cell interaction and bio-mineralization. Apatite is directly in contact with the ECM and interacts freely as soon as the scaffold is implanted. On another hand, matrices produced by jet spraying with an initial blend of HA/PLGA may be a promising system to release progressively HA inside the body. As the same time as the polymer slowly degrades, nanoparticles trapped inside the fibers will be released. By adjusting the fibers diameters and the content of HA, the release of calcium phosphate may be controlled as a drug delivery system (59).

The quality of the minerals deposited or incorporated is well controlled with the jet spray techniques. Nanoparticles do not react chemically during the synthesis process, certifying the composition of the fillers. However, calcium phosphate phases are not fully controlled with SBF mineralization. Calcium deficient (Ca/P ratio lower than 1.67) and NaCl minerals measured by EDX are present on the SBF samples. The *in vitro* mineralization provides less controlled apatite crystals but the final system may be closer as the natural one (presence of amorphous apatite crystals before CaP formation). In the hard tissues of the periodontium, rod-like HA crystals measuring 25-100 nm with a length (c-axis) from 0.1 to 100 µm are present (60). We may control the morphology and dimension of the HA nanoparticles in our study to be as clothe as possible from the biological system.

Further tests should be realized in order to determine the best way to mineralize PLGA nanofibers (cell proliferation viability, adjustments of the production parameters, quality of the fibers, mineralization assays, physical tests, etc.). An additional way, combination of an internal and surface mineralization, has to be explored. A SBF mineralization after a jet spray nanocomposite synthesis or a co jet-spraying synthesis (nHA/PLGA mixture + nHA) will fabricate a system which combines the two advantages of direct surface interaction and progressive calcium release.

Bibliographie

1. *A review on endogenous regenerative technology in periodontal regenerative medicine.* **Fa-Ming Chen, Jing Zhang, Min Zhang, Ying An, Fang Chen, Zhi-Fen Wu.** 2010, Biomaterials, Vol. 31, pp. 7892-7927.

2. *Synthetic biodegradable functional polymers for tissue engineering: a brief review.* **X., GUO BaoLin & MA Peter.** 4, 2014, Science China Chemistry, Vol. 57, pp. 490-500.

3. *Biodegradable polymer matrix nanocomposites for tissue engineering: A review.* **I. Armentano, M. Dottori, E. Fortunati, S. Mattioli, J.M. Kenny.** 2010, Polymer Degradation and Stability, Vol. 95, pp. 2126-2146.

4. Mayo Clinic, medical information and tools for better living.
Mayo Foundation for Medical Education and Research. 2014 [En ligne] www.mayoclinic.com.

5. *Regeneration of periodontal tissues: guided tissue regeneration.* **Villar, Cristina C et Cochran, David L.** 2010, Dental clinincs of North America, Vol. 54, pp. 73-92.

6. *Tissue engineering: From research to dental clinics.* **Vinicius Rosa, Alvaro Della Bona, Bruno Neves Cavalcanti, Jacques Eduardo Nör.** 2012, Dental materials, Vol. 28, pp. 341-348.

7. *Vascularization is the key challenge in tissue engineering.* **Esther C. Novosel, Claudia Kleinhans, Petra J. Kluger.** 2011, Advanced Drug Delivery Reviews, Vol. 63, pp. 300-311.

8. *Poly lactic-co-glycolic acid (PLGA) as biodegradable controlled drug delivery carrier.* **Siegel, Hirenkumar K. Makadia and Steven J.** 2011, Polymers, Vol. 3, pp. 1377-1397.

9. *Alignment of cells and extracellular matrix within tissue-engineered substitutes.* **Jean-Michel Bourget, Maxime Guillemette, Teodor Veres, François A. Auger and Lucie Germain.** 2013, Advances in Biomaterials Science and Biomedical Applications.

10. *A review on polymer nanofibers by electrospinning and their applications in nanocomposites.* **Zheng-Ming Huang, Y.-Z. Zhang, M. Kotaki, S. Ramakrishna.** 2003, Composites Science and Technology, pp. 2223-2253.

11. *Novel and simple alternative to create nanofibrillar matrices of interest for tissue engineering.* **Jérôme Sohier, Pierre Corre, Christophe Perret, Paul Pilet and Pierre Weiss.** 00, 2013, TISSUE ENGINEERING, Vol. 00.

12. *A novel method of selecting solvents for polymer electrospinning.* **C.J. Luo, M. Nangrejo, M. Edirisinghe.** 2010, Polymer, Vol. 51, pp. 1654–1662.

13. *Fabrication of electrospun poly(L-lactide-co-ε-caprolactone)/collagen nanoyarn network as a novel, three-dimensional, macroporous, aligned scaffold for tendon tissue engineering.* **Xu Y, Wu J, Wang H, Li H, Di N, Song L, Li S, Li D, Xiang Y, Liu W, Mo X, Zhou Q.** 2013, Tissue Engineering, Vol. 19.

14. *The potential of anisotropic matrices as substrate for heart valve engineering.* **Jérôme Sohier, Ivan Carubelli, Padmini Sarathchandra, Najma Latif, Adrian H. Chester, Magdi H. Yacoub.** 2013.

15. *Biomimetic mineralization in and on polymers.* **Paul Calvert, Peter Rieke.** 1996, Chemestry of materials, Vol. 8, p. 1715.

16. *Mimicking natural bio-mineralization processes: A new tool for osteochondral scaffold development.* **Anna Tampieri, Simone Sprio, Monica Sandri and Federica Valentini.** 10, 2011, Trends in Biotechnology, Vol. 29.

17. *Biomimetic mineralization.* **An-Wu Xu, Yurong Ma and Helmut Cölfen.** 2007, Journal of Materials Chemistry, Vol. 17, pp. 415-449.

18. *Nanosized hydroxyapatite and other calcium phosphates: Chemistry of formation and application as drug and gene delivery agents.* **Vuk Uskokovic, Dragan P. Uskokovic.** 2011, JOURNAL OF BIOMEDICAL MATERIALS RESEARCH B: APPLIED BIOMATERIALS, Vol. 96B, pp. 152-191.

19. *How useful is SBF in predicting in vivo bone bioactivity?* **Tadashi Kokubo, Hiroaki Takadama.** 2006, Biomaterials, Vol. 27, pp. 2907-2915.

21. *Development of an electrospun nano-apatite/PCL composite membrane for GTR/GBR application.* **Fang Yang, Sanne K. Both, Xuechao Yang, X. Frank Walboomers, John A. Jansen.** 2009, Acta biomaterialia, Vol. 5, pp. 3295-3304.

22. *Bioactivity and Viscoelastic Characterization of Chitosan/Bioglass Composite Membranes.* **Sofia G. Caridade, Esther G. Merino, Natalia M. Alves, Joao F. Mano.** 2012, Macromolecular Bioscience, Vol. 12, pp. 1106-1113.

23. *Formation of bone-like apatite on poly(L-lactic acid) fibers by a biomimetic process.* **Xiaoyan Yuan, Arthur F. T. Mak, Jialu Li.** 2001, John Wiley & Sons.

24. *Biomimetic calcium phosphate coating on electrospun poly(e-caprolactone) scaffolds for bone tissue engineering.* **F. Yang, J.G.C. Wolke, J.A. Jansen.** 2008, Chemical Engineering Journal, Vol. 137, pp. 154-161.

25. *Robocasting nanocomposite scaffolds of poly(caprolactone)/hydroxyapatite incorporating modified carbon nanotubes for hard tissue reconstruction.* **Biligzaya Dorj, Jong-Eun Won, Joong-Hyun Kim,Seong-Jun Choi, Ueon Sang Shin, Hae-Won Kim.** 2012, J Biomed Mater Res.

26. *Development of an electrospun nano-apatite/PCL composite membrane for GTR/GBR application.* **Fang Yang, Sanne K. Both, Xuechao Yang, X. Frank Walboomers, John A. Jansen.** 2009, Acta Biomaterialia, pp. 3295-3304.

27. *Culturing primary human osteoblasts on electrospun poly(lactic-co-glycolic acid) and poly(lactic-co-glycolic acid)/nanohydroxyapatite scaffolds for bone tissue engineering.* **Mengmeng**

Li, Wenwen Liu, Jiashu Sun, Yunlei Xianyu, Jidong Wang, Wei Zhang. 2013, American Chemical Society, Vol. 5, pp. 5921-5926.

28. *Preparation and bioactive properties of novel bone-repair bionanocomposites based on hydroxyapatite and bioactive glassnanoparticles.* **Francisco Valenzuela, Cristian Covarrubias, Constanza Martınez, Patricio Smith, Mario Dıaz-Dosque, Mehrdad Yazdani-Pedram.** 2012, journal of biomedical materials research B: Applied biomaterials, Vol. 100B.

29. *Accelerated bonelike apatite growth on porous polymer/ceramic composite scaffolds in vitro.* **SANG-SOO KIM, MIN SUN PARK, SO-JUNG GWAK, CHA YONG CHOI, and BYUNG-SOO KIM.** 10, 2006, Tissue Engineering, Vol. 12.

30. *Mineralization of hydroxyapatite in electrospun nanofibrous poly(L-lactic acid) scaffolds.* **Jinglu Chen, Benjamin Chu, Benjamin S. Hsiao.** 2006, Journal of Biomedical Materials Research Part A.

31. *A composite of hydroxyapatite with electrospun biodegradable nanofibers as a tissue engineering material.* **Yoshihiro Ito, Hirokazu Hasuda, Masanobu Kamitakahara, Chikara Ohtsuki, Masao Tanihara, Inn-Kyu Kang and Oh Hyeong Kwo.** 1, 2005, JOURNAL OF BIOSCIENCE AND BIOENGINEERING, Vol. 100, pp. 43-49.

32. *Mechanical properties of (poly(L-lactide-co-glycolide))-based fibers coated with hydroxyapatite layer.* **Joanna Buczynska, Elzbieta Pamula, Stanislaw Blazewicz.** 2011, Journal of Applied Polymer Science, Vol. 121, pp. 3702-3709.

33. *Preparation of biomimetic hydroxyapatite by biomineralization and calcination using poly(L-lactide)/gelatin composite fibrous mat as template.* **Qing Cai, Qiaofang Feng, Haiyang Liu, Xiaoping Yang.** 2013, Materials Letters, Vol. 91, pp. 275-278.

34. *Biomineralization of electrospun poly(l-lactic acid)/gelatin composite fibrous scaffold by using a supersaturated simulated body fluid with continuous CO2 bubbling.* **Qing Cai, Qingqing Xu, Qiaofang Feng, Xiaoyan Cao, Xiaoping Yang, Xuliang Deng.** 2011, Applied Surface Science, Vol. 257, pp. 10109-10118.

35. *Poly(lactide-co-glycolide)/hydroxyapatite composite scaffolds for bone tissue engineering.* **Sang-Soo Kim, Min Sun Park, Oju Jeon, Cha Yong Choi, Byung-Soo Kim.** 2005, Biomaterials, Vol. 27, pp. 1399-1409.

36. *The synergistic effect of a hybrid graphene oxide–chitosan system and biomimetic mineralization on osteoblast functions.* 2014, Biomaterials science, Vol. 2, pp. 264-274.

37. *Biomimetic calcium phosphate coating on electrospun poly(e-caprolactone) scaffolds for bone tissue engineering.* **F. Yang, J.G.C. Wolke, J.A. Jansen.** 2008, Chemical Engineering Journal, Vol. 137, pp. 154-161.

38. *Strong and tough mineralized PLGA nanofibers for tendon-to-bone scaffolds.* **Pavan V. Kolluru, Justin Lipner, Wenying Liu, Younan Xia, Stavros Thomopoulos, Guy M. Genin, Ioannis Chasiotis.** 2013, Acta Biomaterialia, pp. 9442-9450.

39. *Nanofiber scaffolds with gradations in mineral content for mimicking the tendon-to-bone insertion site.* **Xiaoran Li, Jingwei Xie, Justin Lipner, Xiaoyan Yuan, Stavros Thomopoulos and Younan Xia.** 7, 2009, Nano Letters, Vol. 9, pp. 2763-2768.

40. *Advanced tissue engineering scaffold design for regeneration of the complex hierarchical periodontal structure.* **Pedro F. Costa, Cedryck Vaquette, Qiyi Zhang, Rui L. Reis, Saso Ivanovski and Dietmar.** 2014, Journal of clinical periodontology, Vol. 41, pp. 283-294.

41. *Amorphous calcium phosphate/poly(D,L-lactic acid) composite nanofibers: Electrospinning preparation and biomineralization.* **Zhao Ma, Feng Chen, Ying-Jie Zhu, Ting Cui, Xuan-Yong Liu.** 2011, Journal of Colloid and Interface Science, Vol. 359, pp. 371-379.

42. *Functionally graded electrospun polycaprolactone and b-tricalcium phosphate nanocomposites for tissue engineering applications.* **Cevat Erisken, Dilhan M. Kalyon, Hongjun Wang.** 2008, Biomaterials, Vol. 29, pp. 4066-4073.

43. *Poly(lactide-co-glycolide)/hydroxyapatite nanofibrous scaffolds fabricated by electrospinning for bone tissue engineering.* **Lihong Lao, Yingjun Wang, Yang Zhu, Yuying Zhang, Changyou Gao.** 2011, Journal of material science, Vol. 22, pp. 1873-1884.

44. *Control of osteogenic differentiation and mineralization of human mesenchymal stem cells on composite nanofibers containing poly[lactic-co-(glycolic acid)] and hydroxyapatite.* **Ji Hye Lee, Nae Gyune Rim, Hyun Suk Jung, Heungsoo Shin.** 2010, Macrobiomolecular Bioscience, Vol. 10, pp. 173-182.

45. *Aligned PLGA/HA nanofibrous nanocomposite scaffolds for bone tissue engineering.* **Moncy V. Jose, Vinoy Thomas, Kalonda T. Johnson, Derrick R. Dean, Elijah Nyairo.** 2009, Acta Biomaterialia, Vol. 5, pp. 305-315.

46. *Influence of ionic strength and carbonate on the Ca-P coating formation from SBFx5 solution.* **F. Barrere, C.A van Blitterswijk, K. de Groot, P. Layrolle.** 2002, Biomaterials, Vol. 23, pp. 1921-1930.

47. *Electrospun biomimetic nanocomposite nanofibers of hydroxyapatite/chitosan for bone tissue engineering.* **Yanzhong Zhang, Jayarama Reddy Venugopal, Adel El-Turki, Seeram Ramakrishna, Bo Su, Chwee Teck Lim.** 2008, Biomaterials, Vol. 29, pp. 4314-4322.

48. *Poly-L-lactic acid/hydroxyapatite hybrid membrane for bone tissue regeneration.* **Gang Sui, Xiaoping Yang, Fang Mei, Xiaoyang Hu, Guoqiang Chen, Xuliang Deng, Seungkon Ryu.** 2007, Journal of Biomedical Materials.

49. *Nanofibrous poly(lactic acid)/hydroxyapatite composite scaffolds for guided tissue regeneration.* **Sung In Jeong, Eun Kyoung Ko, Jungsuk Yum, Chul Ho Jung, Young Moo Lee, Heungsoo Shin.** 2008, Macromolecular Bioscience, Vol. 8, pp. 328-338.

50. *Controllable surface modification of poly(lactic-co-glycolic acid) (PLGA) by hydrolysis or aminolysis I: Physical,chemical, and theoretical aspects.* **Tristan I. Croll, Andrea J. O'Connor, Geoffrey W. Stevens and Justin J. Cooper-White.** 2004, Biomacromolecules, Vol. 5, pp. 463-473.

51. *Materials analysis by X-Ray diffraction, X-Ray fluorescence, atomic absorption, ICP-OES, particle size, surface area, light and scanning electron microscopy and elemental analysis by LSM analytical.* **limited, London & scandinavioan metallurgical Co.** 2006.

52. *Theoritical analysis of calcium phosphate precipitation in simulated body fluid.* **Xiong Lu, Yang Leng.** 2005, Biomaterials, Vol. 26, pp. 1097-1108.

53. *In vitro degradation behavior of electrospun polyglycolide, polylactide, and poly(lactide-co-glycolide).* **Young You, Byung-Moo Min, Seung Jin Lee, Taek Seung Lee, Won Ho Park.** 2005, Journal of applied polymer science, Vol. 95, pp. 193-200.

54. *Nucleation of biomimetic Ca–P coatings on Ti6Al4V from a SBFx5 solution: influence of magnesium.* **F. Barrere, C.A van Blitterswijk, K. de Groot, P. Layrolle.** 2002, Biomaterials, Vol. 23, pp. 2211-2220.

55. *Formation and morphology of asymmetric NaCl particles precipitated at the liquid–liquid interface.* **KAZUNORI KADOTA, YOSHIYUKI SHIRAKAWA∗, IKUMI MATSUMOTO, ATSUKO SHIMOSAKA and JUSUKE HIDAKA.** 06, 2007, Advanced Powder Technol., Vol. 18, pp. 775-785.

56. *Morphology of NaCl crystals in drowning-out precipitation operation.* **H. TAKIYAMA, T. OTSUHATA and M. MATSUOKA.** 1998, Trans IChemE, Vol. 76.

57. *Biomimetic hydroxyapatite coating on pore walls improves osteointegration of poly(L-lactic acid) scaffolds.* **H. Deplaine, M. Lebourg, P. Ripalda, A. Vidaurre, P. Sanz-Ramos, G. Mora, F. Prosper, I. Ochoa, M. Doblare, J. L. Gomez Ribelles, I. Izal-Azcarate, G. Gallego Ferrer.** 2013, JOURNAL OF BIOMEDICAL MATERIALS RESEARCH B: APPLIED BIOMATERIALS, Vol. 101B.

58. *Advanced tissue engineering scaffold design for regeneration of the complex hierarchical periodontal structure.* 2014, Journal of clinical periodontology, Vol. 41, pp. 283-294.

59. *Polymers for drug delivery systems.* **William B. Liechty, David R. Kryscio, Brandon V. Slaughter and Nicholas A. Peppas.** 2012, annual review of chemical and biomolecular engineering.

60. *Calcium phosphate nanoparticles in biomineralization and biomaterials.* **Yurong Cai, Ruikang Tang.** 2008, Journal of materials chemistry.

62. *Fabrication and characterization of multiscale electrospun scaffolds for cartilage regeneration.* **Erica J Levorson, Perumcherry Raman Sreerekha, Krishna Prasad Chennazhi, F Kurtis Kasper, Shantikumar V Nair, and Antonios G Mikos.** 2012, Biomedical Materials, Vol. 8.

63. *Nucleation of biomimetic Ca–P coatings on Ti6Al4V from a SBFx5 solution: influence of magnesium.* **Barrere, F.** 2002, Biomaterials, Vol. 23, pp. 2211-2220.

64. *Controllable surface modification of poly(lactic-co-glycolic acid) (PLGA) by hydrolysis or aminolysis I: physical, chemical, and theoretical aspects.* **Tristan I. Croll, Andrea J. O'Connor, Geoffrey W. Stevens, and Justin J. Cooper-White.** 2004, Biomacromolecules, Vol. 5, pp. 463 - 473.

Annexes

Annex 1- Simulated Body Fluid synthesis protocol

We are largely inspired by the detailed SBF preparation procedure in "How useful is SBF in predicting in vivo bone bioactivity?" Tadashi Kokubo, Hiroaki Takadama. *Biomaterials* 27 (2006) 2907–2915

1) Preparation of SBF 1000mL

Reagents in order:

- (1) Sodium Chloride
- (2) Sodium hydrogen carbonate
- (3) Potassium chloride
- (4) Di-potassium hydrogen phosphate trihydrate
- (5) Magnesium chloride hexahydrate
- (6) 1M (mol/l) Hydrochloric Acid (39mL)
- (7) calcium chloride
- (8) sodium sulfate
- (9) Tris-hydroxymethyl aminomethane
- (10) 1M (mol/l) Hydrochloric Acid (0-5mL)
- Distilled water

Materials:
- 2000mL Plastic beaker
- Magnetic stirring
- pH meter/thermocouple
- Cylinder (HCl)
- Serynge/ drop wise for HCl
- 2000 ml volumetric flask
- 104 x 50mL plastic beaker
- Water bath

Precautions:

- Always make sure that the preparing solution is kept colourless and transparent and that there is no deposit on the surface of the bottle. If any precipitation occurs, stop preparing SBF, abandon the solution, restart from washing the apparatus and prepare SBF again.

1. Put 700 mL of ion-exchanged and distilled water with a stirring bar into 1000mL plastic beaker. Heat the water in the beaker to 36.5 +/-1.5°C under stirring.
2. Dissolve only the reagents of 1st to 8th order into the solution at 36.5 +/-1.5 °C one by one in the order given previously, taking care of the indications in the following list.
    - Never dissolve several reagents simultaneously. Dissolve a reagent only after the preceding one (if any) is completely dissolved.
    - Measure the volume of 1M-HCl (39mL) by cylinder after washing with 1M-HCl.
    - Measure the hygroscopic reagents such as KCl, K2HPO4 3H2O, MgCl2 6H2O, CaCl2, Na2SO4 in as short a period as possible.
3. Set the temperature of the solution at 36.5+/-1.5 °C. If the amount of the solution is smaller than 900 ml, add ion exchanged and distilled water up to 900ml in total.
4. Insert the electrode of the pH meter into the solution. Just before dissolving the Tris, the pH of the solution should be 2.0+/-1.0
5. With the solution temperature between 35 and 38 °C, preferably to 36.5+/-0.5 °C, dissolve the reagent Tris into the solution little by little taking careful note of the pH change. After adding a small amount of Tris, stop adding it and wait until the reagent already introduced is dissolved completely and the pH has become constant; then add more Tris to raise the pH gradually. When the pH becomes 7.30+/-0.05, make sure that the temperature of the solution is maintained at 36.5+/-0.5 °C. With the solution at 36.5+/-0.5 °C, add more Tris to raise the pH to under 7.45.
    - Do not add a large amount of Tris into the solution at a time, because the radical increase in local pH of the solution can lead to the precipitation of calcium phosphate. If the solution temperature is not within 36.5+/-0.5 °C, add Tris to raise the pH to 7.30+/-0.05, stop adding it and wait for the solution temperature to reach 36.5+/-0.5 °C.

- The pH shall not increase over 7.45 at 36.5+/-0.5 °C, taking account of the pH decrease with increasing solution temperature (the pH falls about 0.05/°C at 36.5+/-1.5 °C).

6. When the pH has risen to 7.45+/-0.01, stop dissolving Tris, then drop 1M-HCl by syringe to lower the pH to 7.42+/-0.01, taking care that the pH does not decrease below 7.40. After the pH has fallen to 7.42+/-0.01, dissolve the remaining Tris little by little until the pH has risen to <=7.45. If any Tris remains, add the 1M-HCl and Tris alternately into the solution. Repeat this process until the whole amount of Tris is dissolved keeping the pH within the range of 7.42–7.45. After dissolving the whole amount of Tris, adjust the temperature of the solution to 36.5+/-0.2 °C. Adjust the pH of the solution by dropping 1M-HCl little by little at a pH of 7.42/+-0.01 at 36.5+/-0.2 °C and then finally adjust it to 7.40 exactly at 36.5 °C on condition that the rate of solution temperature increase or decrease is less than 0.1 °C/min. Remove the electrode of the pH meter form the solution, rinse it with ion-exchanged and distilled water and add the washings into the solution.
7. Put the pH-adjusted solution from the beaker into 1000 ml volumetric flask. Rinse the surface of the beaker with ion-exchanged and distilled water and add the washings into the flask several times, fixing the stirring bar with a magnet as if to prevent it from falling into the volumetric flask. Add the ion-exchanged and distilled water up to the marked line (it is not necessary to adjust exactly, because the volume becomes smaller after cooling), put a lid on the flask and close it with plastic film. After mixing the solution in the flask, keep it in the water to cool it down to 20 °C. After the solution temperature has fallen to 20 1C, add the distilled water up to the marked line.
8. Prepared SBF should be preserved in a plastic bottle with a lid put on tightly and kept at 5-10 °C in a refrigerator. The SBF shall be used within 30 days after preparation.

2) NaOH activation

a. With the help of a synthetic paintbrush, spread at the surface of the PLGA matrix a small amount of NaOH [0.01M].
   For reproducibility reasons: two ways trip?
b. Wait for a specific time (see tables)
c. Wash with demineralized water

3) SBF immersion

a. When they are completely dry, put PLGA samples (100 mm^2) into a 50mL plastic beaker containing the SBF solution (around 40mL).
   PLGA film hold by welding two opposite sample corners to the top of the plastic flask
b. Wait for different time (see tables)
c. Wash 3 times with demineralized water

Annex 2 - Determination of the adequate SBF volume for a good sample immersion

Based on Kukubo's paper work, we calculate the appropriate volume of SBF needed to mineralize in good conditions the PLGA samples (1cmx1cm).

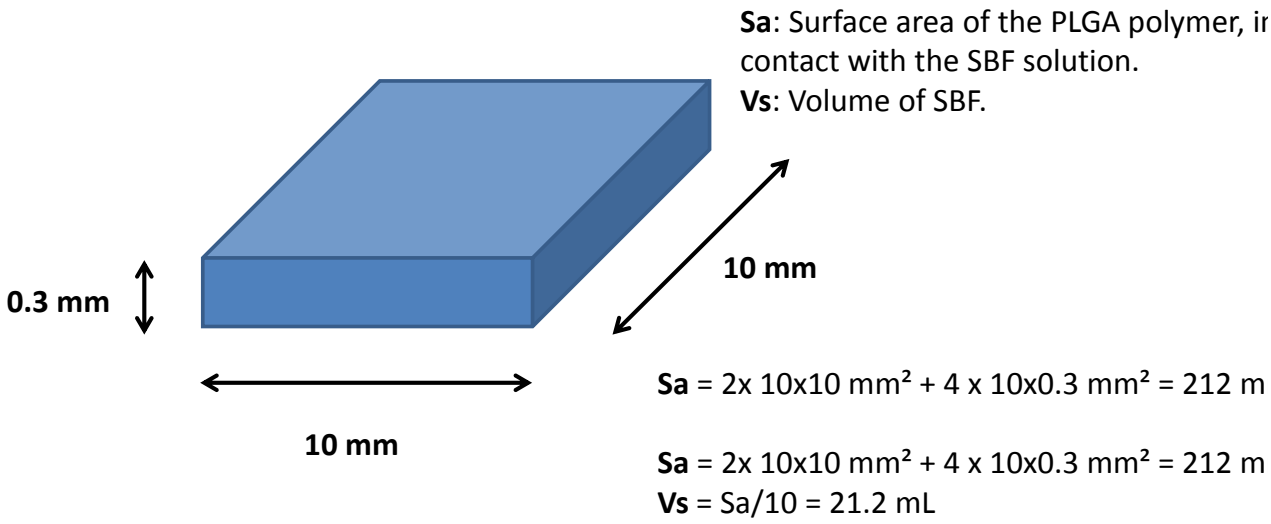

Figure 11 – PLGA sample dimensions

As the surface area is higher with porous materials, we have to increase the SBF volume. The forecasted porosity of the polymer (activated with 0.01M NaOH solution) is ~49.6%. We will multiply the previous calculated volume by a factor of 2.

A final SBF volume of 40mL for each 100mm² PLGA samples was selected.